Enhancing the Accuracy and Generality of the Debye–Grüneisen Model: Optimizing the Volume Dependence for Accurate Predictions Across Varied Compositions

Yi Wang[1,2]; Xingru Tan[3]; Saro San [1,2]; Shanshan Hu[3]; Michael C. Gao[1]

[1]National Energy Technology Laboratory, 1450 Queen Avenue SW, Albany, OR 97321, USA
[2]NETL Support Contractor, 1450 Queen Avenue SW, Albany, OR 97321, USA
[3]Mechanical & Aerospace Engineering Department, Benjamin M. Statler College of Engineering and Mineral Resources, West Virginia University, Morgantown, WV 26505, USA

Abstract

In this work we have introduced an optimized Debye-Grüneisen model that revolutionizes the determination of the Debye temperature and Grüneisen parameters. Unlike conventional methods, our model requires only the 0 K energy volume data for a material as input, eliminating the need to determine the bulk modulus and its pressure derivative, which often pose challenges due to numerical uncertainties. This unique feature sets our model apart from existing approaches and streamlines the process, enabling accurate predictions of thermal expansion behavior across various materials. To demonstrate its effectiveness, we showcase its excellent agreement with measured coefficients of thermal expansion (CTE) for the nickel-cobalt-chromium-aluminum-yttrium (Ni-Co-Cr-Al-Y) bond-coating system. Additionally, we apply our approach by conducting a high-throughput search for potential bond-coating materials among 90,000 compositions within the aluminum-cobalt-chromium-iron-nickel (Al-Co-Cr-Fe-Ni) system. From this extensive search, four compositions are synthesized, and the measured CTE values agree very well with theoretical predictions, hence validating our approach. The current optimized Debye-Grüneisen model combined with Density Functional Theory (DFT)-based thermodynamic database enables reliable and efficient high-throughput calculations of CTE of Ni-based alloys without expensive phonon calculations.

Keywords: Debye-Grüneisen model; Density functional theory; Bond coating materials; Coefficient of thermal expansion; Debye temperature; Grüneisen parameters

1 Introduction

Density Functional Theory (DFT) 1,2 is a quantum mechanical method utilized for predicting electronic and ground-state properties of materials. It relies on the concept of total electron density, derived from solving the Kohn-Sham[1] equations. Regular DFT computations are typically conducted at 0 K, offering valuable insights into various material characteristics, including total energy, electronic density of states, and interatomic force constants.

However, many applications require predictions of a material's thermodynamic properties at finite temperatures. Within the framework of DFT, two common approaches are often considered: the quasi-harmonic phonon approach[3,4], where interatomic force constants are typically calculated at 0 K, and the Debye-Grüneisen approach[5,6], which requires only the 0 K static energy volume as input. The phonon approach, based on lattice dynamics, is highly accurate in determining vibrational free energy for mechanically stable solids. However, the phonon approach is computationally demanding and often struggles to address the effects, such as intrinsic anharmonic effects that go beyond the quasi-harmonic approximation, along with issues of imaginary phonon

frequencies in high-temperature phases of some materials that are mechanically unstable at 0 K [7]. Since this research primarily aims to predict the coefficients of thermal expansion (CTE) for complex high-entropy materials, phonon calculations are considered too computationally expensive.

In contrast, the Debye–Grüneisen approach offers a simplified alternative for calculating the vibrational free energy contribution. Although its computational cost requirements are negligible compared to the phonon approach, its current implementation may sacrifice some accuracy for efficiency. This compromise stems from uncertainties in determining important input parameters such as the Debye temperature and the Grüneisen parameters. For example, one may need to resort to using an artificial scaling factor for the Debye temperature[5], and there has been ambiguity in the expressions for the Grüneisen parameters, with variations among the Slater[8], Dugdale-MacDonald[6], and Vashchenko-Zubarev[9] expressions. For instance, Kang et al. [10] found that the high-temperature entropy-derived Debye temperature used for phase diagrams can differ from the low-temperature elastic-constant or heat-capacity-derived Debye temperature by a factor of 0.94. Music et al. [11] used low-temperature elastic constants to calculate the Debye temperature, while Ma et al. [12] applied the bulk modulus as proposed by Moruzzi et al. [5], along with Slater's high-temperature Grüneisen parameters, for the CoCrFeMnNi high-entropy alloy system. A further inspiration for this work is to circumvent the uncertainty arising from fitting DFT numerical data using the equation of state [13,14]. An additional consideration is to calibrate the parameters resulting from the choice of DFT functionals, which can contribute significantly to this uncertainty in certain cases.

The primary objective of this work is to address these challenges by developing an optimized model that enhances the accuracy of the Debye-Grüneisen approach while minimizing its associated uncertainties. We aim to create a robust methodology to determine the Debye temperature and the Grüneisen parameter accurately, thereby improving the predictive power and applicability of the Debye-Grüneisen model. This optimized model integrates the volume dependence of the Grüneisen parameter within the Debye-Grüneisen framework, eliminating the need for researchers to determine additional parameters beyond the 0 K energy-volume data.

This advancement enables the utilization of DFT outputs through two methods:

i) Direct Method: This approach predicts a material's thermodynamic properties solely based on 0 K energy-volume data. Additionally, it facilitates the construction of thermodynamic databases used in the indirect method. This procedure has been applied to build a thermodynamic database using the energy-volume data obtained from previous work[15] on over 3,000 atomic structures involving 26 elements, including Al, boron(B), carbon (C), Cr, copper (Cu), hafnium (Hf), lanthanum (La), manganese (Mn), molybdenum (Mo), nitrogen (N), niobium (Nb), oxygen (O), phosphorus (P), rhenium (Re), ruthenium (Ru), sulfur (S), silicon (Si), tantalum (Ta), titanium (Ti), vanadium (V), tungsten (W), Y, and zirconium (Zr).

ii) Indirect Method: This method utilizes the thermodynamic database from the direct method to rapidly predict a material's thermodynamic properties, eliminating the need for specific DFT calculations for the material. Consequently, it enables high-throughput predictions of a material's thermodynamic properties across various compositions.

These advancements streamline the application of DFT in thermodynamic calculations and establish a robust theoretical framework for understanding and predicting material behavior under diverse thermodynamic conditions, including variations in temperature and pressure.

The structure of this work is as follows: In Section 2, the direct approach is detailed, covering the optimized Debye-Grüneisen model and the procedure for computing the CTE using the energy-volume curve as the sole input, alongside the establishment of a DFT database. Section 3 introduces the indirect approach, which allows for the prediction of the CTE for a material of specified composition. This approach leverages an existing DFT database, obviating the requirement for additional DFT calculations. Section 4 showcases the proposed methodologies by comparing their predictions with experimental data. Finally, Section 5 presents the conclusions drawn from the present research findings.

2 Direct DFT Approach

2.1 Calculate CTE by DFT when the Helmholtz Free Energy is Readily Available

For a given material, if the Helmholtz free energy as a function of both temperature and volume is known, thermal expansion can be directly estimated by observing the increase in equilibrium volume along the Helmholtz free energy versus volume curve as temperature rises. At a specific temperature, the equilibrium volume is typically determined by minimizing the Helmholtz free energy with respect to volume. For isotropic materials, the equilibrium length of the sample can be calculated as the cubic root of the equilibrium volume. The linear CTE can then be estimated as the first derivative of the equilibrium length with respect to temperature, divided by the equilibrium length.

Nowadays, it has become routine to use DFT to estimate the Helmholtz free energy by[16,17]

$$F(V,T) = E_c(V) + F_{vib}(V,T) + F_{el}(V,T) \qquad \text{Eq. 1}$$

In this formulation, $F(V,T)$ represents the Helmholtz free energy per atom at a given volume V and temperature T; E_c is the static total energy at 0 K; F_{vib} is the vibrational contribution; and F_{el} is the thermal electronic contribution that can be calculated based solely on the electronic density of states. A detailed description of the formulation for F_{el} can be found in the referenced prior works[4,16,17].

In this work, we aim to determine F_{vib} in Eq. 1 by improving the Debye-Grüneisen approach[5]. In this approach, the expression of the vibrational free energy follows:

$$F_{vib}(V,T) = \frac{9}{8}k_B\Theta_D(V) + k_BT\left\{3\,ln\left[1 - exp\left(-\frac{\Theta_D(V)}{T}\right)\right] - D\left(\frac{\Theta_D(V)}{T}\right)\right\} \qquad \text{Eq. 2}$$

where k_B represents the Boltzmann's constant, D is the Debye function, and the Debye temperature $\Theta_D(V)$ is expressed as:

$$\Theta_D(V) = \Theta_0\left(\frac{V_0}{V}\right)^{\gamma} \qquad \text{Eq. 3}$$

where Θ_0 represents the Debye temperature at the 0 K static equilibrium volume V_0, which is the zero-pressure volume point obtained from the DFT energy versus volume curve and γ is the so-called Grüneisen parameter, which is the focus of the next subsections.

2.2 Volume Dependence of the Grüneisen Parameter

In the original Debye-Grüneisen model proposed by Moruzzi et al. [5], the Grüneisen parameter γ in Eq. 3 is often treated as a constant under zero-pressure conditions. However, this approximation does not hold well if temperature range is wide, especially for materials with high anharmonicity, such as Mo and W[6]. To improve the accuracy of the Grüneisen parameter expression, researchers have explored various approaches. For instance, to model the pressure dependence of the melting temperature, Burakovsky and Preston[18] proposed treating γ as an analytic function of $V^{1/3}$, capturing the effects of volume changes more realistically.

In this work, we propose to reconsider the volume dependence of the Grüneisen parameter to improve the agreement with experiment if involving wide temperature range. After making a few tries, an excellent solution is found to express the volume dependence as:

$$\gamma(V) = \gamma_0 \left(\frac{V}{V_0}\right)^{\delta} \qquad \text{Eq. 4}$$

Here, γ_0 represents the Grüneisen parameter at the 0 K static equilibrium volume V_0, which is the zero-pressure volume point obtained from the DFT energy versus volume curve, and δ is a constant which is referred to as the Grüneisen exponent. This formulation is inspired by the expression of the Debye temperature in Eq. 3, which relates the Debye temperature to the relative volume (V/V_0) in the power form.

By introducing this expression for the volume dependence of the Grüneisen parameter, we achieve a more accurate and realistic depiction of its behavior with respect to volume changes, particularly in capturing intrinsic anharmonic effects beyond the quasiharmonic approximation. This refinement enhances the accuracy in describing thermodynamic properties, addressing limitations in Moruzzi's Debye-Grüneisen model[5], which treats the Grüneisen parameter as a constant.

2.3 Calibrating the Parameters for Pure Elements

A preliminary test was conducted using this approach to calculate the δ parameter through the phonon model for highly anharmonic systems, such as Mo and W. However, the results were unsatisfactory, likely due to the phonon model's limited ability to fully capture intrinsic anharmonic effects.

Alternatively, for pure elements or species commonly used as reference systems with abundant experimental data, we accordingly calibrated the parameter Θ_0, γ_0, and δ to reproduce the experimental CTE, aided by the calculated energy-volume curves at 0 K by DFT. During the process of calibrating the parameters, Θ_0, γ_0, and δ, the thermodynamic calculations have been performed using the Density Functional Theory Took Kit (DFTTK) package[19]. The calibrated Debye temperature and Grüneisen parameters for a selection of 28 pure elements, including silver (Ag), Al, gold (Au), C, cadmium (Cd), Co, Cr, Cu, Fe, Hf, magnesium (Mg), Mn, Mo, Nb, Ni, lead (Pb), platinum (Pt), Re, antimony (Sb), Si, tin (Sn), Ta, Ti, V, W, Y, zinc (Zn), and Zr, are collected in Table 1 where the equilibrium atomic volume V_0 calculated by DFT in this work is also listed.

Indeed, when treating $\delta = 0$ in Eq. 4, the Grüneisen parameter from the optimized model becomes a constant, thus recovers the result by Moruzzi et al.,[5] who treat the Grüneisen parameter as a constant. However, as indicated in Table 1, the values of δ for the 28 pure elements obtained from

the optimized model are significantly different from zero, ranging from negative value of -0.3061 for Fe to 5.6326 for C (diamond). These far from zero values of δ imply the importance of the volume dependence of the Grüneisen parameter.

To demonstrate the ability of the optimized approach, Figure 1 showcases the comparison between the calculated CTE based on the calibrated parameters and experimental CTE using Al, Co, Cr, Ni, Fe, and Hf. These figures demonstrate the success of Eq. 4 for the accurate description of CTE. Additional data for the CTEs of the elements Ag, Au, C, Cd, Cu, Mg, Mn, Mo, Nb, Pb, Pt, Re, Sb, Si, Sn, Ta, Ti, V, W, Y, Zn, and Zr are presented in Figure S1 in the supplementary materials.
Being different from the original Debye-Grüneisen model proposed by Moruzzi et al., the Grüneisen parameter by the optimized Debye-Grüneisen model is no longer a constant. To avoid confusion and maintain clarity in terminology, we propose introducing an effective Grüneisen parameter based on the logarithmic derivative of the Debye temperature with respect to the logarithm of the volume. Aided by Eq. 3 and Eq. 4, we obtain:

$$\gamma_{eff} = \gamma_0 \left(\frac{V}{V_0}\right)^{\boldsymbol{\delta}} \left[1 + \delta ln\left(\frac{V}{V_0}\right)\right] \qquad \text{Eq. 5.}$$

Using Al, Co, Cr, Ni, Fe, and Hf, Figure 2 showcases a comparison between the effective Grüneisen parameters obtained from the optimized Debye-Grüneisen model and the Grüneisen parameters determined by the Slater[8], Dugdale-MacDonald[6], and Vashchenko-Zubarev[9] expressions. Additional data for the Grüneisen parameters of the element Ag, Au, C, Cd, Cu, Mg, Mn, Mo, Nb, Pb, Pt, Re, Sb, Si, Sn, Ta, Ti, V, W, Y, Zn, and Zr are presented in Figure S2 supplied in the supplementary materials.

It is observed that the Grüneisen parameters obtained from the optimized Debye-Grüneisen model naturally span from the low-temperature values derived from the Dugdale-MacDonald or Vashchenko-Zubarev expressions to the high-temperature values derived from the Slater expression. The optimized Debye-Grüneisen model thus resolves the ambiguity for users in selecting the appropriate expression for the Grüneisen parameter when applying Moruzzi's Debye-Grüneisen model. Consequently, the optimized Debye-Grüneisen model provides a consistent and continuous representation of the Grüneisen parameter, ensuring a smoother transition between different temperature regimes and capturing a more comprehensive temperature range of material behavior.

2.4 Determining Parameters for Compounds

To apply the Debye-Grüneisen model to a compound, the most challenging aspect is how to accurately determine the Debye temperature and Grüneisen parameter, considering ambiguity and precision. In this study, we propose a procedure to determine the Debye temperature while adhering to Eq. 3 and Eq. 4. We propose to determine the parameters Θ_0, γ_0, and δ for a compound through the geometric average of those obtained for the constituent pure elements or species discussed in the previous subsection. Doing so eliminates the ambiguities for the determinations of Θ_0, γ_0, and δ for each specific composition. The procedures are given below:

We propose to determine Θ_0 for a compound in Eq. 3 by:

$$\Theta_0 = \prod_i \left[\Theta_0(i)\left(\frac{V_0(i)}{V_0}\right)^{\gamma(i)}\right]^{x_i} \quad \text{Eq. 6}$$

where Θ_0 represents the 0 K Debye temperature of the compound, $\Theta_0(i)$ represents the 0 K Debye temperature of the element or species *i*, $V_0(i)$ represents the 0 K equilibrium atomic volume of the element or species *i*, and V_0 represents the 0 K equilibrium atomic volume of the compound. Here we note that the term $\left(\frac{V_0(i)}{V_0}\right)^{\gamma(i)}$ in Eq. 6 accounts for a volume correction to the Debye temperature of an element when its environment changes from the pure element to the compound; in other words, the atomic volume of the element is modified to the average atomic volume within the compound.

The variable x_i in Eq. 6 denotes the normalized composition of the compound, and $\gamma(i)$ in Eq. 6 is the Grüneisen parameter for the element or species *i*, given by the following equations:

$$\gamma(i) = \gamma_0(i)\left(\frac{V_0}{V_0(i)}\right)^{\boldsymbol{\delta}(i)} \quad \text{Eq. 7}$$

where $\gamma_0(i)$ represents the Grüneisen parameter at the equilibrium volume of the element or species *i* and $\delta(i)$ represents the Grüneisen exponent of the element or species *i*. Here again, the term $\left(\frac{V_0}{V_0(i)}\right)^{\boldsymbol{\delta}(i)}$ serves as a volume correction when the environment changes from the pure element to the compound.

Following the scheme of the geometric average, the Grüneisen parameter and Grüneisen exponent of a compound can be determined, respectively, by:

$$\gamma_0 = \prod_i [\gamma(i)]^{x_i} \quad \text{Eq. 8}$$

and

$$\delta = \prod_i [\delta(i)]^{x_i} \quad \text{Eq. 9}$$

This geometric averaging approach provides a way to account for the contributions of individual elements or species in determining the overall properties of the compound.

2.5 True CTE vs Mean CTE

It is worth mentioning that there are two types of definitions for linear CTE, the true (differential) CTE and the mean (average) CTE[20]. The true CTE, mostly used by the theoreticians, corresponds to the first derivative of the curve of the linear thermal expansion with respect to the temperature, by:

$$\alpha_T = \frac{1}{L(T)}\frac{dL(T)}{dT} \quad \text{Eq. 10}$$

Here, $L(T)$ represents the length of the sample as a function of temperature.

The mean CTE, mostly used by the experimentalists, is defined as the slope of a secant through two points of the curve of linear thermal expansion, by:

$$\alpha_M = \frac{1}{L(298.15)} \frac{L(T) - L(298.15)}{T - 298.15} \quad \text{Eq. 11}$$

In this equation, $L(298.15)$ represents the initial length of the sample at 298.15 K.

2.6 Building the DFT Database

With this procedure, a comprehensive thermochemical database is constructed based on the previous high-throughput first-principles calculations of energy versus volume curves and electronic density of states, over 3,000 atomic structures (containing mainly the binary and ternary and a few quaternary compounds) for Ni, Fe, and Co alloys with Al, B, C, Cr, Cu, Hf, La, Mn, Mo, N, Nb, O, P, Re, Ru, S, Si, Ta, Ti, V, W, Y, and Zr[21].

The database includes both the stoichiometric crystalline phases, the disordered phases (treated with special quasirandom structure (SQS) approach[22-24]), and the dilute solution phases as listed in Table 2. For the magnetic structures, Co, Fe, and Ni are treated as ferromagnetic. Antiferromagnetic states for Cr and Mn are treated with supercell containing two Cr and 58 Mn atoms, respectively.

The thermodynamic data collected in the database include temperature, atomic volume, Gibbs energy, entropy, enthalpy, linear CTE, heat capacities, bulk modulus, and more as a function of temperature.

2.7 Details of DFT Calculations

The DFT calculations were performed using the Vienna Ab initio Simulation Package (VASP)[25]. The projector augmented wave (PAW-PBE) potentials under the generalized gradient approximation (GGA) for exchange-correlation potential was utilized[26,27]. Convergence tolerance of 10^{-6} eV was utilized for electronic relaxation while the tolerance of 10^{-4} eV was utilized for structural relaxation. For structural relaxation, we employed the first-order Methfessel-Paxton method with a Gaussian smearing of 0.2 eV for Brillouin zone integration, in addition to the default energy cutoff determined with the VASP key setting of "PREC=accurate". Following the structural relaxation, high-accuracy total energy calculations were conducted using Blöch's tetrahedron method, employing a plane wave expansion with an energy cutoff of 400 eV. The *k*-points mesh was determined based on a reciprocal density of 5,000 points per atom.

3 Indirect/High-Throughput DFT Approach to Calculate CTE

When the need arises to determine the CTEs for hundreds or even thousands of materials within a time scale of minutes, employing the direct DFT approach for CTE calculations becomes unfeasible. This section outlines an alternative indirect approach for predicting the CTE of a given material, utilizing the database described in the previous section. With this method, our objective is to estimate the CTE of a specific material within the timespan of just one-tenth of a second, relying solely on its composition. The procedure is as follows:

Let us use $\overline{C_j}(j = 1, \dots, n)$ to represent the overall atomic composition of a given *n*-component system, where *j* indexes the element in the system. For such a system, we can employ the Dantzig algebra[28], following the previous work[21], to calculate its phase equilibrium. The phase fractions as a function of temperature are predicted by performing a constrained minimization of the following objective function in terms of the Gibbs free energy, which at zero pressure equals to the Helmholtz free energy at equilibrium volume:

$$G(T) = \sum_{\sigma=1}^{m} f^{\sigma}(T) G^{\sigma}(T) \qquad \text{Eq. 12}$$

Here, G^{σ} represents the Gibbs energy per atom of phase σ, m is the number of phases, and f^{σ} is the phase fraction of the σth phase. The minimization with respect to f^{σ} subjects to the following two conditions:

$$\overline{C_j} = \sum_{i=\sigma}^{m} f^{\sigma}(T) x_j^{\sigma} \qquad \text{Eq. 13}$$

where x_j^{σ} represents the composition of the *j*th element in the σth phase, and

$$\sum_{\sigma=1}^{m} f^{\sigma}(T) = 1 \qquad \text{Eq. 14}$$

At the given temperature, two important outcomes from the above minimization process are:

i) if f^{σ}equals to one at σ = *k* and all other $f^{\sigma}(\sigma \neq k)$ equal to zero, it means that the system will be stable at the single phase *k*; and
ii) Otherwise, if more than one f^{σ}'s are not zero, the system will consist of a mixture of multiple phases with f^{σ} being the phase fraction of the corresponding phase.

For a system made of multiple phases, we can approximate the CTE as:

$$\bar{\alpha} = \sum_{\sigma=1}^{m} f^{\sigma}(T) \frac{V^{\sigma}}{\bar{V}} \alpha^{\sigma} + \sum_{\sigma=1}^{m} \frac{df^{\sigma}(T)}{dT} \frac{V^{\sigma}}{\bar{V}} \qquad \text{Eq. 15}$$

For the calculations performed in this work, the term $\frac{df^{\sigma}(T)}{dT}$ has been neglected, as it only becomes significant near the phase transition temperature, where the CTE exhibits considerable uncertainty. The variable V^{σ} in Eq. 15 is the atomic volume of σth phase, and α^{σ} is the CTE of the σth phase that can be computed using Eq. 1 with Eq. 10 or Eq. 11. $\bar{V}$ in Eq. 15 is the averaged atomic volume of the system:

$$\bar{V} = \sum_{\sigma=1}^{m} f^{\sigma}(T) V^{\sigma} \qquad \text{Eq. 16}$$

4 Results and Discussions

4.1 Benchmark Calculation

Verification of both the direct and indirect DFT approaches has been carried out using the bond coating materials of NiCo17Cr14AlY and NiCoCrAlY, and the superalloy René N5, for which experimental data are available from studies by Haynes et al.,[29] and Taylor and Walsh[30]. CTE is a key consideration for bond coating to ensure optimal performance and durability of the coated structure. René N5 is a high-performance material[31] known for its excellent mechanical properties, particularly at high temperatures. It's commonly used in aerospace applications, such as in jet engines and gas turbines. René N5 is typically made of the γ (gamma) phase, which is the face centered cubic (FCC) phase of Ni.

In particular for the direct DFT calculations, these three alloys have been treated as random FCC alloys with the SQS approach[22-24]. The comparisons between the predictions and experimental data from Haynes et al.,[29] and Taylor and Walsh[30] are depicted in Figure 3. It is notable that the experimental data fall neatly between the predicted CTEs obtained from both direct and indirect DFT calculations. The moderate volume jumps observed in the indirect DFT calculations stem from the discontinuous changes in phase fractions associated with the indirect approach. The observed discrepancy between predicted CTEs from the indirect approach and those from the direct approach can be partly attributed to the neglect of the sudden volume jump across phase transition due to the usage of Eq. 15.

4.2 Verification of the Indirect DFT Approach

To support the proposed indirect DFT approach, we conducted CTE calculations for two series of alloy systems, as documented by Haynes et al.,[29] and by Taylor and Walsh[30]. The comparison with the measured CTEs, specifically the mean CTE, reported by Haynes et al.,[29] for Ni10Cr19AlY, Ni20Cr19AlY, NiCo17Cr14Al, and Ni7Cr13AlY is presented in Figure 4. Additionally, a comparison with the measured CTEs reported by Haynes et al., for Ni25Al+Hf, Ni40Al, Ni50Al+Hf, and Ni50Al is shown in Figure 5. Furthermore, we compared the predicted CTEs with the measured values reported by Taylor and Walsh[30] for a set of alloys (the compositions of these alloys are listed in Table 3), and these comparisons are illustrated in Figure 6 and Figure 7.

From these comparisons, it can be confidently asserted that the agreement between the predictions and experimental measurements is outstanding. The kinks observed along the CTE curves represent phase transitions. In sum, these comparisons serve to demonstrate the capability of the proposed optimized Debye-Grüneisen model to accurately predict the thermal expansion behavior of complex materials.

4.3 High-Throughput Screening for Bond Coating Material

Being able to efficiently predict the CTE across a wide range of compositions and temperatures is invaluable for materials research, especially for applications like searching for potential bond coating materials. By utilizing the indirect approach outlined in Section 3, researchers can expedite the screening process and analyze a vast number of compositions. This approach enables efficient exploration of a larger design space and can lead to the rapid discovery of novel materials with desirable properties. We applied this methodology to search for a potential bond coating material within the Al-Co-Cr-Fe-Ni system among 90,000 compositions for target application temperatures from 1000 °C to 1200 °C.

Remarkably, these predictions can be completed within the scale of an hour of a standard central processing unit (CPU). The predicted CTEs for the 90,000 compositions by the indirect approach are provided in the supplementary materials as csv files.

4.4 Experimental and Direct DFT Verification for the High-Throughput Screening Result

In this work, we have selected four compositions, $Al_{16}Co_{18}Cr_{14}Fe_{18}Ni_{34}$, $Al_{20}Co_{18}Cr_{16}Fe_{18}Ni_{28}$, $Al_{22}Co_{18}Cr_{6}Fe_{10}Ni_{44}$, and $Al_{26}Co_{10}Cr_{10}Fe_{6}Ni_{48}$ for experimental validation. These compositions were chosen to undergo direct DFT calculations and synthesized for conducting CTE measurements.

4.4.1 Experimental Setups for the Measurements of CTE

The alloy ingots for experiment validation were synthesized via arc-melting using high-purity (99.99 wt.%) Al, Co, Cr, Fe, Ni metals, and reactive elements Y and Hf. The elemental blend was melted five times on a water-cooled Cu hearth under a Ti-gettered high-purity argon atmosphere to ensure compositional homogeneity, then cast into ingots measuring 2" × 2.5" × 0.5".

For the assessment of oxidation resistance, square plates (10 mm × 10 mm × 3 mm) were sectioned from the cast ingots using electrical discharge machining (EDM). Samples underwent metallographic preparation, involving grinding with silicon carbide (SiC) papers followed by polishing with 0.05 μm colloidal alumina. Prior to oxidation testing, samples were rigorously cleaned with acetone and air-dried. For testing, samples were placed in alumina crucibles which have been pre-oxidized at 1150 °C for over 1,000 hours to prevent additional oxidation weight gain during evaluation. The discontinuous oxidation experiment was performed at 1150 °C in a chamber furnace under atmosphere environment for up to 1000 h, with exposure intervals of 100 h. The procedure included ramping the furnace temperature to 1150 °C, then swiftly inserting the samples and exposing them for 100 h, and then turning off the furnace, letting the samples cool down to room temperature before removing them from the furnace. The weight of the samples is measured twice, with and without the crucible, using a analytical balances with 0.01 mg precision.

The phase composition of the alloy and oxide scale was studied using X-ray diffraction (XRD) in a diffractometer (X'Pert Pro, PANalytical, the Netherlands) fitted with Cu Kα radiation at 45 kV. The spectra were collected in the 2θ range of 20∼100 degree, with a step size of 0.02 degree, and a scanning speed of 0.5 degree/min. The microstructure and chemical composition of samples were examined using scanning electron microscopy (SEM) (JEOL JSM-7600F, Japan) equipped with energy dispersive X-ray spectroscopy (EDS).

The CTE for each alloy was measured using 5 × 5 × 10 (mm) specimens. Specimens were tested in a Netzsch (Burlington, MA) DIL 402 CL dilatometer using an alumina push rod with a pushing load force of 200 mN. The measurement temperature ramp from 50 °C to 1300 °C with a heating rate of 2 °C/min. The measurements were conducted under flowing argon gas with flow rate of 50 ml/min to inhibit oxidation.

4.4.2 Experimental Results

For these four compositions, the CALculation of PHAse Diagrams (CALPHAD) method[32] was employed to determine the phase fractions using TCNI8 database, revealing that they consisted exclusively of FCC and B2 phases within the interested temperature range from 1000 °C to 1200 °C. Subsequently, direct DFT calculations were conducted for both the FCC and B2 phases

using the SQS approach. In this method, it should mention that the B2 phase was treated with two sublattices, utilizing the site compositions obtained from the CALPHAD analysis.

In Figure 8, the calculated CTEs are compared with the measurements. The calculated CTEs are derived as an average between the FCC phase and B2 phase, utilizing the respective phase fractions (between parenthesis in each subplots) given in each figure panel of Figure 8, estimated by CALPHAD at 1150 °C. To mitigate the impact of significant data uncertainty arising from the measurements, a smoothing process was applied. The collected data underwent averaging over temperature intervals of 150 °C.

Post-CTE microstructure analysis (see Figure S2 in the Supplementary Materials) revealed no evidence of precipitation, segregation, or the formation of additional phases in any of the four HEA samples, underscoring their phase stability during CTE measurement. Supporting this, XRD analysis (see Figure S3 in the Supplementary Materials) indicated consistent structural integrity across all samples post-CTE, with no detectable formation of new phases or significant changes in phase distribution. Minor α-alumina peaks were observed, likely due to minimal oxidation from trace oxygen (ppm levels) in the argon gas used during CTE measurement. However, this oxidation is negligible, as all four samples exhibit strong alumina-forming properties, creating dense, protective α-alumina layers that provides excellent oxidation resistance.
DSC analysis over the temperature range of 80 °C to 1450 °C was conducted to confirm the absence of phase transitions during CTE measurements, indicating that the alloys maintained structural stability. The observed bumps in CTE values, as shown in Figure 8, are thus attributed to shifts in phase fractions rather than discrete phase transformations. XRD results corroborate a general trend of increasing FCC content and decreasing BCC content across all alloys post-CTE, consistent with compositional shifts without altering primary phase stability.
In particular, post-CTE micrographs (see Figure S3-S8 in the Supplementary Materials) illustrate this phase evolution within the $Al_{16}Co_{18}Cr_{14}Fe_{18}Ni_{34}$ alloy, where a notable increase in a 'needle-like' phase was observed. This needle-like morphology is attributed to the growth of an Al-poor FCC phase, emphasizing the alloy's tendency for compositional redistribution under thermal cycling conditions without compromising the bulk structure. Together, these findings confirm the high thermal and structural stability of the alloys, even in the presence of minor oxidation, and underscore the robust phase consistency of the HEAs under study.

For high temperature applications, CTE is a very important property parameter to minimize thermal stress due to the mismatch in CTE between joint components or between base alloys and coatings. Experiments show that a low mismatch in CTE between the bond coating and α-Al_2O_3 at 1150 °C leads to significantly longer service time against spallation[29]. It is intuitively expected that low CTE values would contribute to lower creep rate of an alloy in general. The present work addressed the urgent need in developing reliable and efficient models in predicting CTE for wide ranges of alloy compositions. Our optimized Debye-Grüneisen approach considers the volume dependence of the Grüneisen parameter, and excellent agreement is achieved between model prediction and experiments for a variety of alloy compositions. Furthermore, the current optimized Debye-Grüneisen model combined with DFT-based thermodynamic database enables robust high-throughput calculations of CTE of Ni-based alloys and hence greatly accelerates high-temperature alloy design.

1. Summary

In conclusion, this paper presents an optimized Debye-Grüneisen model that simplifies the determination of the Debye temperature and Grüneisen parameters. By requiring only the 0 K energy volume data for a material as input, this model eliminates the need to determine the bulk modulus and the pressure derivative of the bulk modulus, overcoming challenges associated with numerical uncertainties and setting itself apart from existing models. Through this streamlined process, our optimized Debye-Grüneisen model enables accurate predictions of thermal expansion behavior across various materials.

Our study demonstrates the effectiveness of the optimized model by showcasing its excellent agreement with measured CTE for the Ni-Co-Cr-Al-Y bondcoat system. Additionally, we validate the approach through a rigorous process, conducting a high-throughput search for potential bondcoat materials among 90,000 compositions within the Al-Co-Cr-Fe-Ni system. Meticulously screening compositions based on criteria such as CTE and corrosion resistance, we synthesize and measure four compositions, demonstrating excellent agreement with theoretical predictions.

The optimized model offers versatile applications: researchers capable of computing the energy-volume curve using DFT can directly predict the CTE. Conversely, for materials with arbitrary compositions, the CTE can be predicted without performing DFT calculations for them. This is achieved by utilizing a comprehensive database compiled from pre-existing DFT calculations, providing a valuable tool for expedited material property prediction and exploration.

In summary, our optimized Debye-Grüneisen model presents a novel and robust approach to thermal expansion prediction, enhancing accuracy across a wide range of materials. Its effectiveness is evidenced by the excellent agreements with measured CTE for both the Ni-Co-Cr-Al-Y and Al-Co-Cr-Fe-Ni systems, establishing a promising avenue for future research in material science and engineering.

Looking ahead, the versatility of this optimized Debye-Grüneisen model offers promising applications. For researchers equipped with DFT capabilities, it provides a direct pathway to predict CTE with minimal computational effort. For those working with arbitrary or new compositions, predictions can be made using a comprehensive DFT-based database, offering a rapid and cost-effective means of material exploration and property prediction.

Authors' Contributions

The project was conceived by Michael C. Gao and Shanshan Hu. The writing was carried out by Yi Wang, the calculations and data generation were carried out by Yi Wang and Saro San, Yi Wang proposed the methodology, and Xingru Tan performed the CTE measurements. All authors actively engaged in the discussion and interpretation of the results and contributed to the final writing of the manuscript. The final manuscript was thoroughly edited and proofread by all authors.

Data Availability Statement

All data are listed in tables or presented in figures in the main text or Supplementary Material.

Disclaimer

This project was funded by the United States Department of Energy, National Energy Technology Laboratory, in part, through a site support contract. Neither the United States Government nor any agency thereof, nor any of their employees, nor the support contractor, nor any of their employees, makes any warranty, express or implied, or assumes any legal liability or responsibility for the accuracy, completeness, or usefulness of any information, apparatus, product, or process disclosed, or represents that its use would not infringe privately owned rights. Reference herein to any specific commercial product, process, or service by trade name, trademark, manufacturer, or otherwise does not necessarily constitute or imply its endorsement, recommendation, or favoring by the United States Government or any agency thereof. The views and opinions of authors expressed herein do not necessarily state or reflect those of the United States Government or any agency thereof.

Acknowledgements

The authors acknowledge financial support from the Department of Energy's (DOE) Office of Energy Efficiency and Renewable Energy (EERE) through award DE-EE0010214, “High-Entropy Alloy-Based Coating to Protect Critical Components in Hydrogen Turbine Power System”. This research used the resources of the National Energy Research Scientific Computing Center, a DOE Office of Science User Facility supported by the Office of Science of the U.S. Department of Energy under NERSC awards ALCC-ERCAP0022624 and ALCC-ERCAP0029917, and computational resources sponsored by the U.S. DOE's Office of Energy Efficiency and Renewable Energy and located at the National Renewable Energy Laboratory.

Conflict of Interest

The authors declare there is no conflict of interest.

References

1 Kohn, W., , Sham, L. J. & SELF-CONSISTENT EQUATIONS INCLUDING EXCHANGE AND CORRELATION EFFECTS. *Phys. Rev.* **140**, A1133-1138 (1965).

2 Hohenberg, P., , Kohn, W. & Inhomogeneous Electron Gas. *Phys. Rev.* **136**, B864-B871 (1964).

3 Giannozzi, P. *et al.* QUANTUM ESPRESSO: a modular and open-source software project for quantum simulations of materials. *J. Phys. Condens. Matter* **21**, 395502 (2009).

4 Wang, Y. *et al.* A first-principles approach to finite temperature elastic constants. *J. Phys. Condens. Matter* **22**, 225404 (2010). https://doi.org:10.1088/0953-8984/22/22/225404

5 Moruzzi, V. L., Janak, J. F. & Schwarz, K. Calculated thermal properties of metals. *Physical Review B* **37**, 790-799 (1988). https://doi.org:10.1103/PhysRevB.37.790

6 Wang, Y. *et al.* Mean-field potential approach to the quasiharmonic theory of solids. *Int. J. Quantum Chem.* **96**, 501-506 (2004). https://doi.org:10.1002/qua.10769

7 Parlinski, K., Li, Z. & Kawazoe, Y. First-principles determination of the soft mode in cubic ZrO 2. *Physical Review Letters* **78**, 4063 (1997).
8 Slater, J. C. & *Introduction to chemical physics*. (Read Books Ltd, 2011).
9 Vashchenko, V. Y. & Zubarev, V. Concerning the Grüneisen constant. *Sov. Phys. Solid. State* **5**, 653-655 (1963).
10 Tang, K., Wang, T., Qi, W. & Li, Y. Debye temperature for binary alloys and its relationship with cohesive energy. *Physica B: Condensed Matter* **531**, 95-101 (2018).
11 Music, D., Geyer, R. W. & Keuter, P. Thermomechanical response of thermoelectrics. *Applied Physics Letters* **109** (2016).
12 Ma, D., Grabowski, B., Körmann, F., Neugebauer, J. & Raabe, D. Ab initio thermodynamics of the CoCrFeMnNi high entropy alloy: Importance of entropy contributions beyond the configurational one. *Acta Materialia* **100**, 90-97 (2015).
13 Guan, P.-W., Houchins, G. & Viswanathan, V. Uncertainty quantification of DFT-predicted finite temperature thermodynamic properties within the Debye model. *The Journal of Chemical Physics* **151** (2019).
14 Shang, S.-L. *et al.* First-principles thermodynamics from phonon and Debye model: Application to Ni and Ni3Al. *Comput. Mater. Sci.* **47**, 1040-1048 (2010). https://doi.org:10.1016/J.COMMATSCI.2009.12.006
15 Wang, Y. *et al.* A thermochemical database from high-throughput first-principles calculations and its application to analyzing phase evolution in AM-fabricated IN718. *Acta Materialia* **240**, 118331 (2022). https://doi.org:https://doi.org/10.1016/j.actamat.2022.118331
16 Wang, Y. *et al.* Thermodynamic properties of Al, Ni, NiAl, and Ni3Al from first-principles calculations. *Acta Mater.* **52**, 2665-2671 (2004). https://doi.org:10.1016/J.ACTAMAT.2004.02.014
17 Wang, Y. *et al.* Calculated equation of state of Al, Cu, Ta, Mo, and W to 1000 GPa. *Phys. Rev. Lett.* **84**, 3220 (2000).
18 Burakovsky, L. & Preston, D. L. Analytic model of the Grüneisen parameter all densities. *Journal of Physics and Chemistry of Solids* **65**, 1581-1587 (2004).
19 Wang, Y. *et al.* DFTTK: Density Functional Theory ToolKit for high-throughput lattice dynamics calculations. *Calphad* **75**, 102355 (2021). https://doi.org:10.1016/J.CALPHAD.2021.102355
20 Holcomb, G. R. & A review of the thermal expansion of magnetite. *Mater. High Temp.* **36**, 232-239 (2019).
21 Wang, Y. *et al.* Computation of entropies and phase equilibria in refractory V-Nb-Mo-Ta-W high-entropy alloys. *Acta. Mater.* **143** (2018). https://doi.org:10.1016/j.actamat.2017.10.017
22 van de Walle, A. *et al.* Efficient stochastic generation of special quasirandom structures. *Calphad* **42**, 13-18 (2013). https://doi.org:10.1016/J.CALPHAD.2013.06.006
23 Zunger, A. *et al.* Special quasirandom structures. *Phys. Rev. Lett.* **65**, 353-356 (1990).
24 Shin, D. *et al.* First-principles study of ternary fcc solution phases from special quasirandom structures. *Phys. Rev. B* **76**, 144204 (2007).
25 Kresse, G. & Furthmüller, J. Efficiency of ab-initio total energy calculations for metals and semiconductors using a plane-wave basis set. *Computational materials science* **6**, 15-50 (1996).

26 Kresse, G. *et al.* From ultrasoft pseudopotentials to the projector augmented-wave method. *Phys. Rev. B Condens. Matter* **59**, 1758-1775 (1999).
27 Perdew, J. P. *et al.* Generalized Gradient Approximation Made Simple. *Phys. Rev. Lett.* **77**, 3865-3868 (1996).
28 Dantzig, G. B. *et al.* The generalized simplex method for minimizing a linear form under linear inequality restraints. *Pacific J. Math.* **5**, 183-195 (1955).
29 Haynes, J., Pint, B., Porter, W. & Wright, I. Comparison of thermal expansion and oxidation behavior of various high-temperature coating materials and superalloys. *Mater. High Temp.* **21**, 87-94 (2004).
30 Taylor, T. & Walsh, P. Thermal expansion of MCrAlY alloys. *Surf. Coat. Technol.* **177**, 24-31 (2004).
31 Wang, R. *et al.* Microstructure characteristics of a René N5 Ni-based single-crystal superalloy prepared by laser-directed energy deposition. *Additive Manufacturing* **61**, 103363 (2023).
32 Andersson, J. O. *et al.* Vol. 26 273-312 (2002).
33 Zhang, B., Li, X. & Li, D. Assessment of thermal expansion coefficient for pure metals. *Calphad* **43**, 7-17 (2013).
34 Touloukian, Y. S., Kirby, R., Taylor, R. & Desai, P. *Thermal expansion: metallic elements and alloys*. (IFI/Plenum, 1975).
35 *Thermal Expansion Coefficient of Metals & Materials | Toolbox | AMERICAN ELEMENTS ®*, <https://www.americanelements.com/thermal-expansion-coe.html> (

5 Figures and Tables

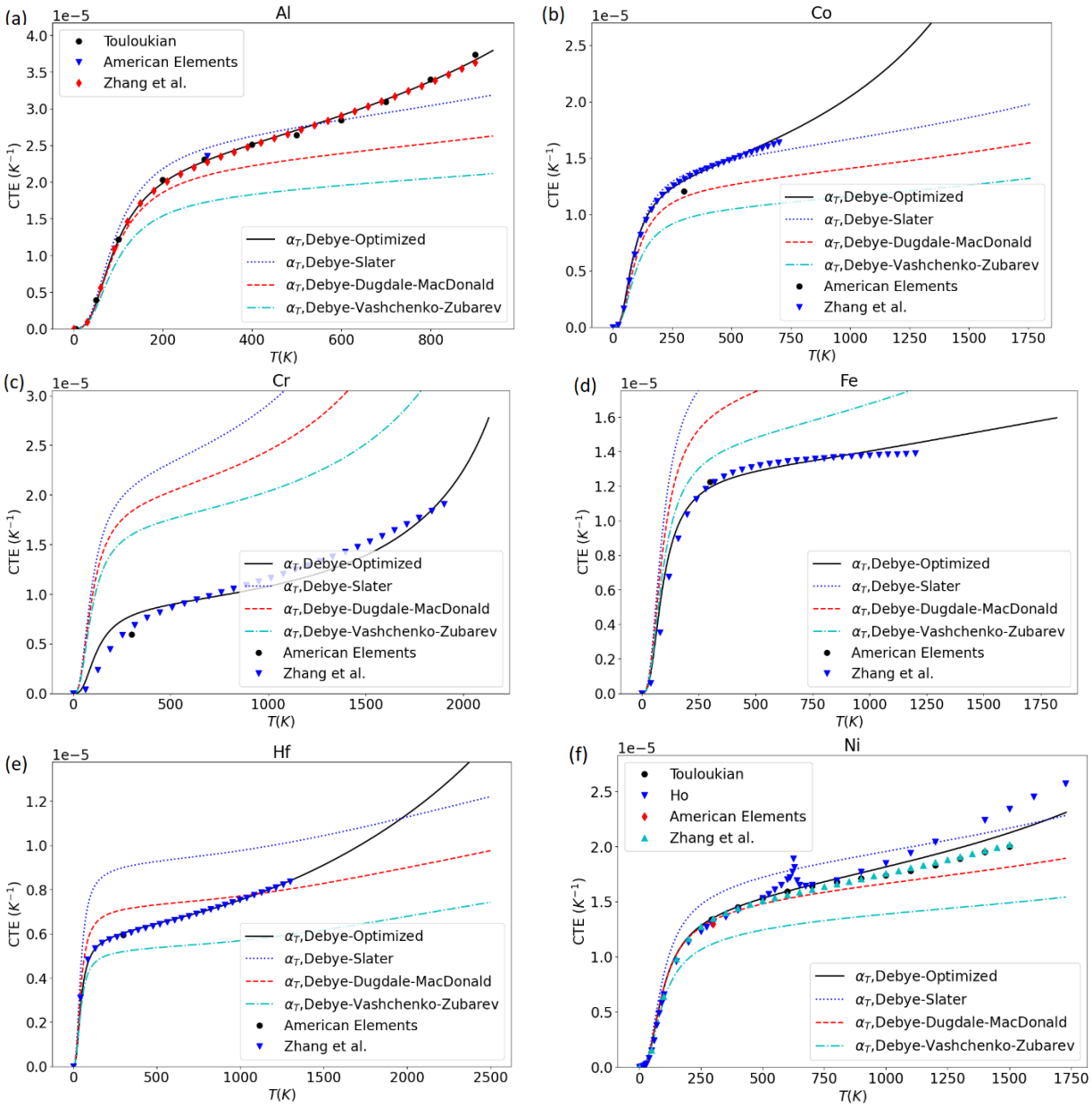

Figure 1: Comparison of the true linear coefficient of thermal expansion (α_T) described by the present optimized Debye-Grüneisen model with the Moruzzi model[5] employing the Grüneisen parameters determined by the Slater[8], Dugdale-MacDonald[6], and Vashchenko-Zubarev[9] expressions. The dots plotted in the left panels represent the experimental CTEs for pure elements[33-35]: (a) Al, (b) Co, (c) Cr, (d) Fe, (e) Hf, and (f) Ni.

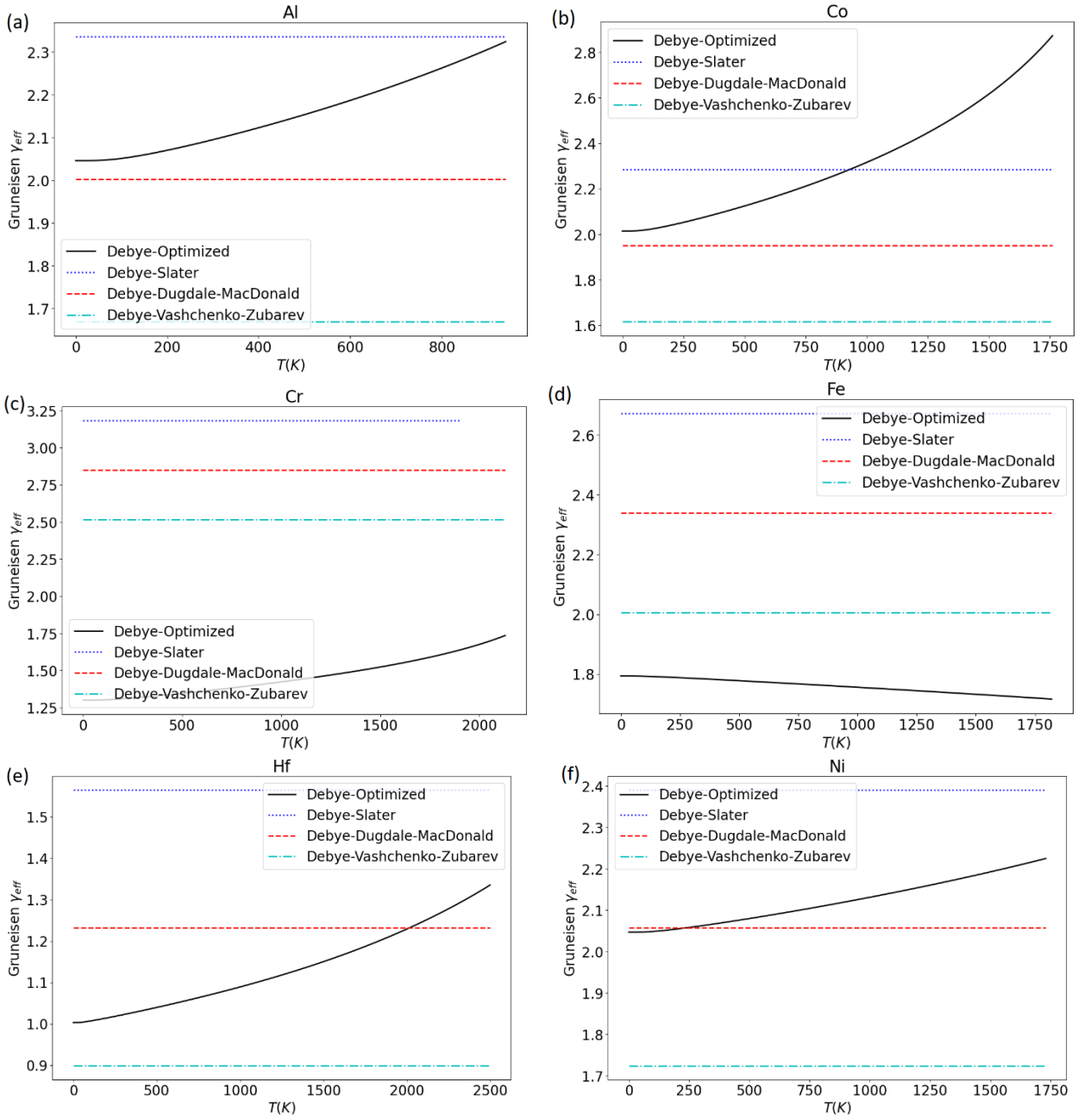

Figure 2: The effective Grüneisen parameters (γ_{eff}, see Eq. *5* in the main text) as described by the present optimized Debye-Grüneisen model. For comparison, the Grüneisen parameters calculated using the expressions by the Slater[8], Dugdale-MacDonald[6], and Vashchenko-Zubarev[9] are also shown for (a) Al, (b) Co, (c) Cr, (d) Ni, (e) Fe, and (f) Hf.

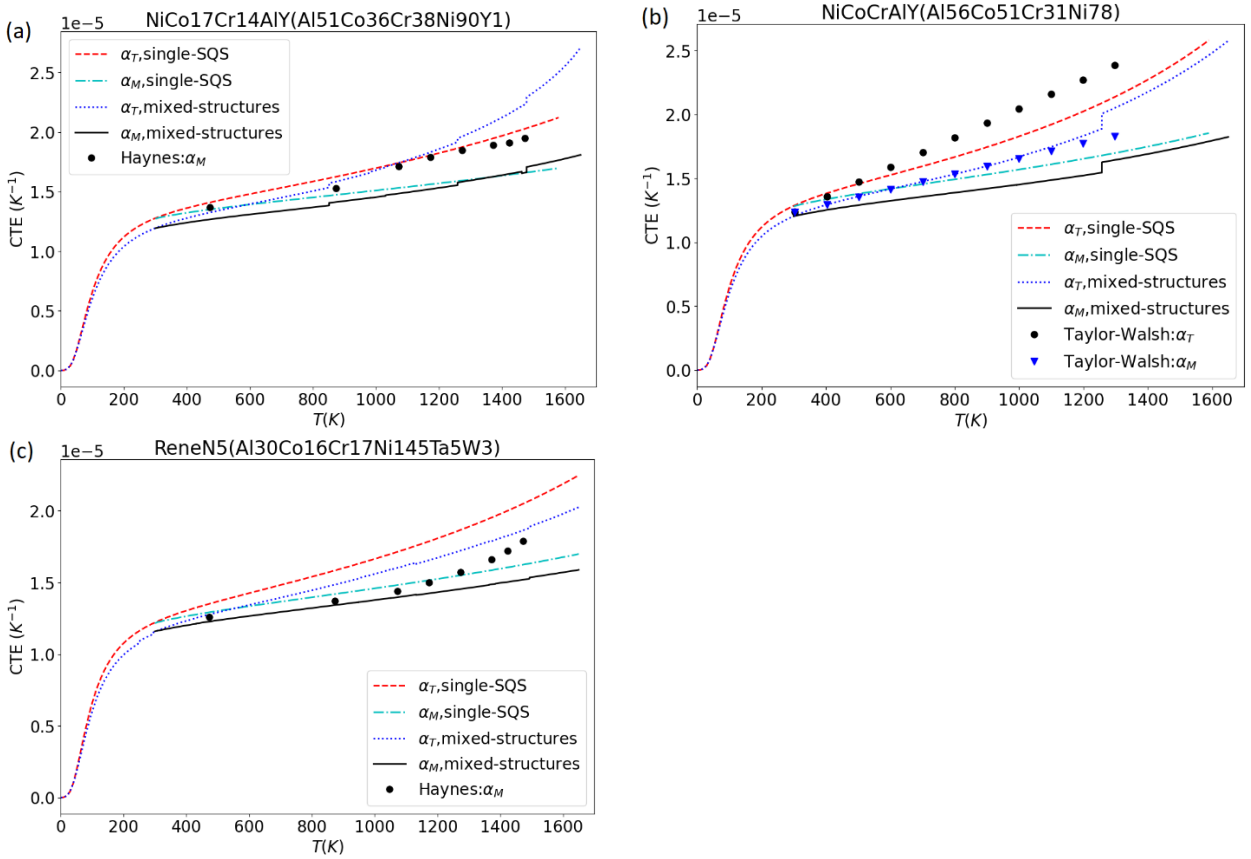

Figure 3: Comparison of the linear CTEs predicted by the optimized Debye-Grüneisen model with the measured CTEs for selected benchmark materials of (a) NiCo17Cr14AlY, (b) NiCoCrAlY, and (c) René N5. The dots represent the experimental data from Haynes et al.[29] and Taylor and Walsh[30]. The dotted line represents the mean CTE calculated by the direct DFT approach using single SQS structure, the solid line represents the instant CTE calculated by the direct DFT approach using single SQS structure, the long dashed line represents the mean CTE calculated by the indirect DFT approach (see Section 3), and the dot-dashed line represents the instant CTE calculated by the indirect DFT approach (see Section 3).

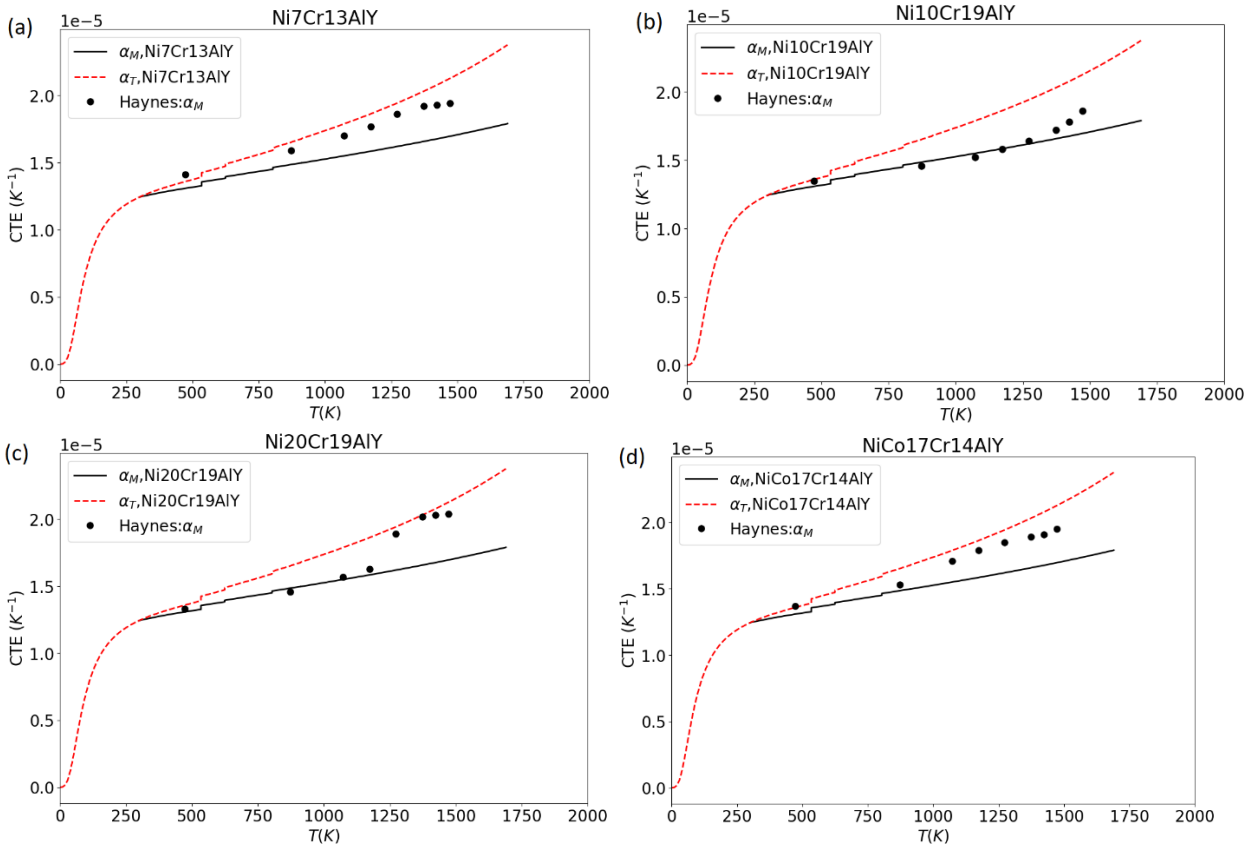

Figure 4: Comparison of the liner CTEs predicted by the optimized Debye-Grüneisen model with the measured CTEs for the Ni-Co-Cr-Al-Y system by Haynes et al.[29].

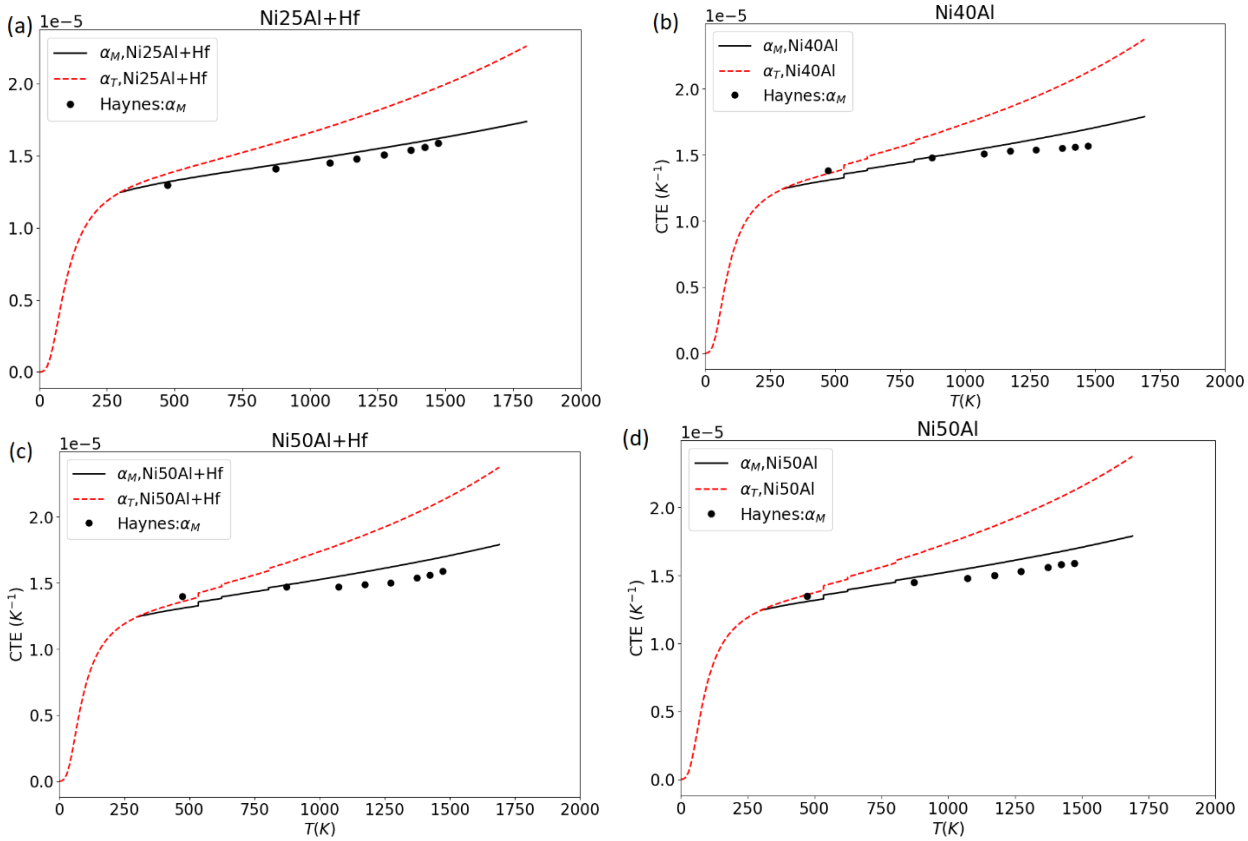

Figure 5: Comparison of the linear CTEs predicted by the optimized Debye-Grüneisen model with the measured CTEs for the Ni-Al system by Haynes et al.[29].

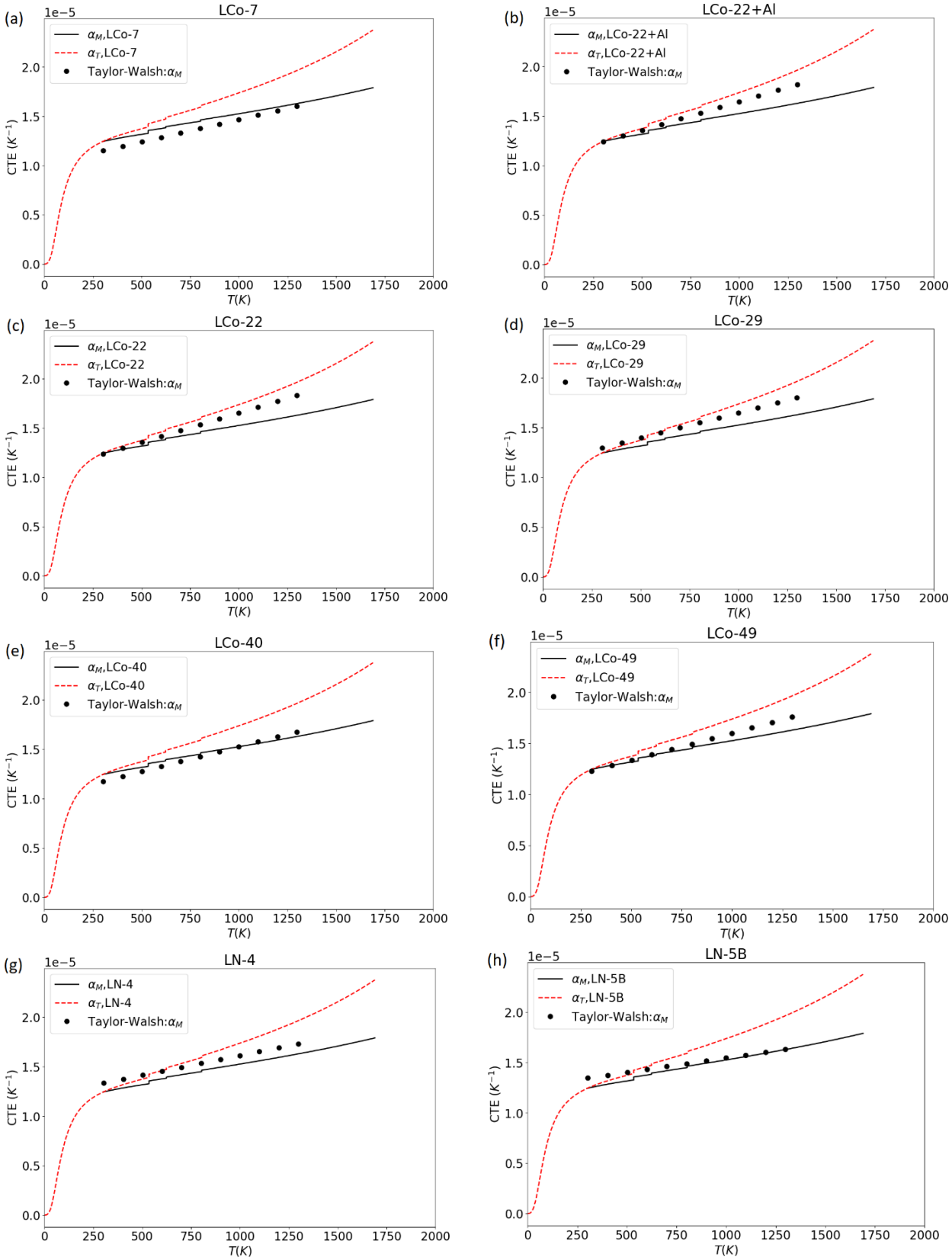

Figure 6: Comparison of the linear CTEs predicted by the indirect approach with the measured CTEs by Taylor and Walsh[30].

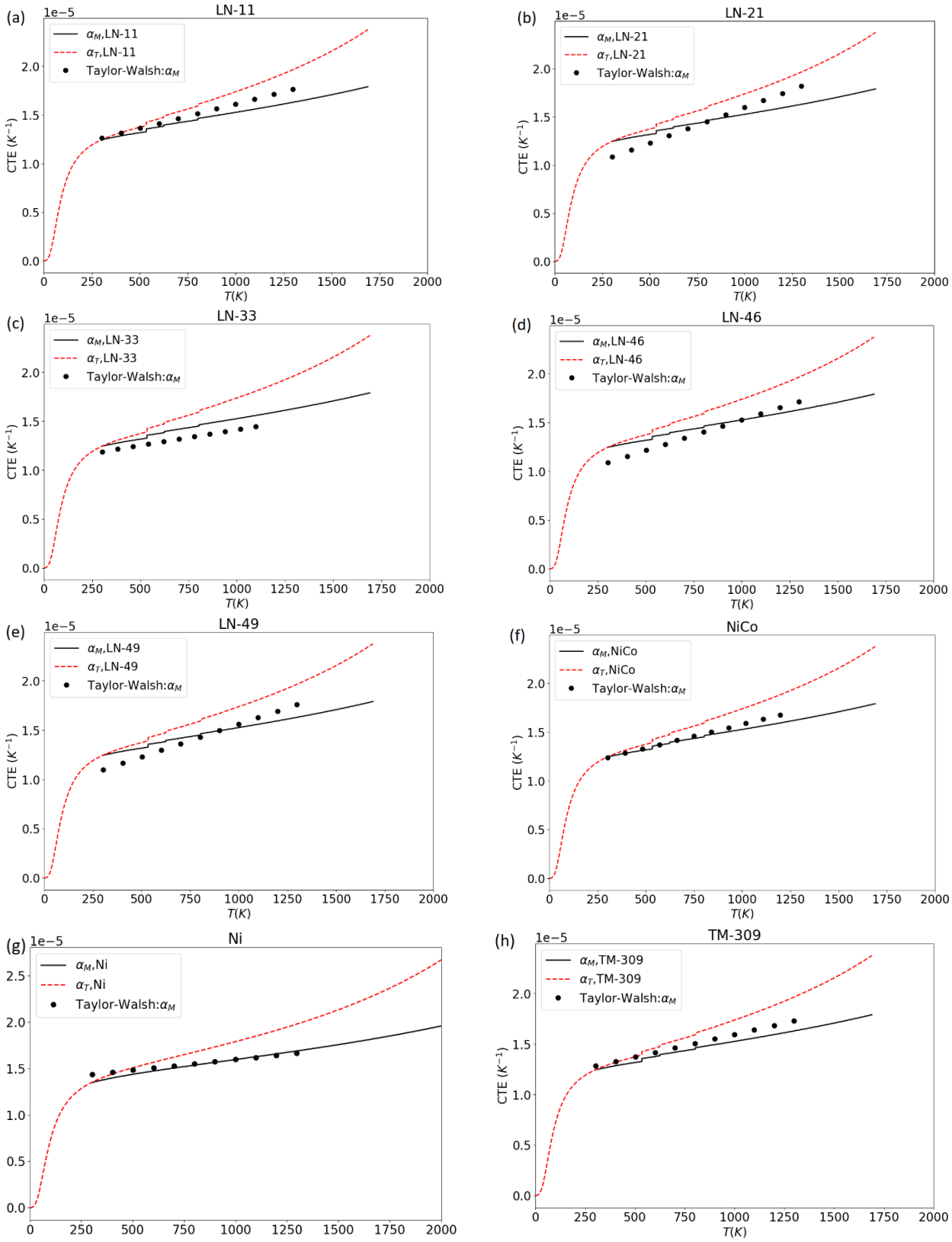

Figure 7: Comparison of the linear CTEs predicted by the indirect approach with the measured CTEs by Taylor and Walsh[30].

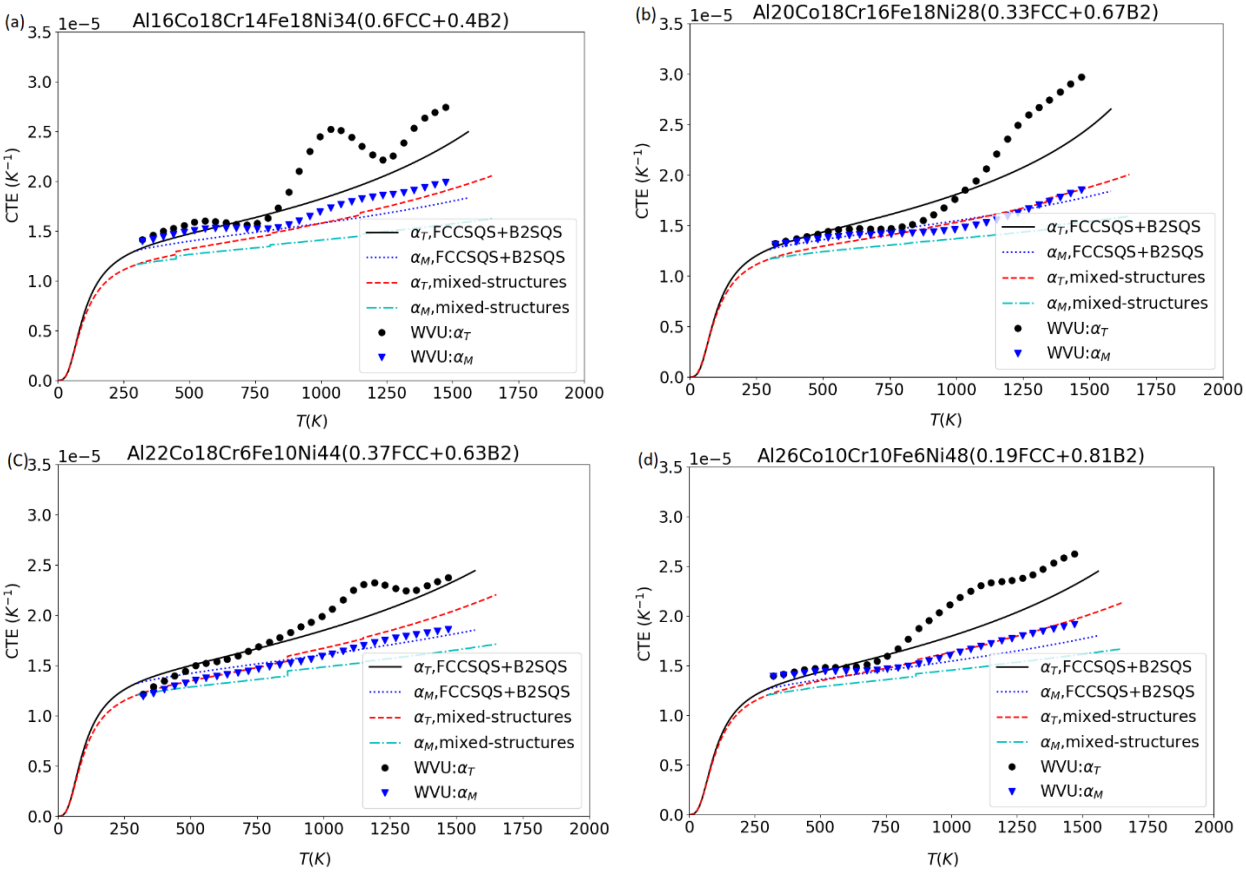

Figure 8: The comparison of the linear CTEs predicted by the optimized Debye-Grüneisen model with the measured CTEs of this work for the four compositions within the Al-Co-Cr-Fe-Ni system. In the graph, experimental data points are denoted by dots. The dotted line represents the mean CTE calculated using the direct DFT approach, determined as a weighted average between the FCC and B2 phases. Conversely, the solid line represents the instantaneous CTE calculated using the direct DFT approach, obtained again by a weighted average between the FCC and B2 phases. The long dashed line represents the mean CTE calculated by the indirect DFT approach (see Section 3) and the dot-dashed line represents the instant CTE calculated by the indirect DFT approach (see Section 3). The numbers between parenthesis are phase fractions at 1150 °C obtained from CALPHAD approach using TCNI8 database.

Table 1: Calibrated Parameters (Refer to Eq. 3 and Eq. 4 and Associated Notes for their Definitions) for the Optimized Debye-Grüneisen Model, Alongside the DFT Equilibrium Atomic Volume at 0 K (V_0) for Selected Pure Elements

Element	Θ_0 (K)	γ_0	δ	V_0 (Å^3/atom)
Ag	218.08	2.1103	0.4486	17.8484
Al	392.03	2.0108	0.9283	16.4676
Au	175.27	2.4249	0.7783	17.9583
C	1615.6	0.5762	5.6326	5.7068
Cd	130.6	1.7327	0.3923	23.0563
Co	356.02	1.9813	1.6945	10.8095
Cr	506.47	1.2781	1.9289	11.8436
Cu	322.98	1.932	0.6662	12.0183
Fe	380.63	1.7992	−0.3061	11.378
Hf	186.79	0.998	2.2638	22.4418
Mg	322.64	1.37	1.0325	22.9086
Mn	390.26	3.2397	1.7662	11.0853
Mo	333.39	1.3904	3.1012	15.756
Nb	287.33	1.5835	0.2444	18.1155
Ni	395.76	2.035	0.4897	10.8666
Pb	90.81	2.2911	0.7807	31.9081
Pt	233.61	2.293	0.9573	15.6064
Re	287.33	2.5247	0.5422	14.9315
Sb	180.26	0.6417	−0.7596	31.9165
Si	814.81	0.434	4.874	20.4463
Sn	155.75	1.6454	2.8147	28.412
Ta	213.56	1.4078	2.4935	18.321
Ti	349.95	1.1881	1.4772	17.3724

V	394.84	1.4753	1.4026	13.4901
W	312.2	1.6224	1.9152	15.9379
Y	240.46	0.9587	0.6664	32.8007
Zn	210.28	1.7363	−0.3987	15.3875
Zr	251.04	0.8885	3.1579	23.4251

Table 2: Ordered and Disordered Structures included in the Database

Structure	Range of Elements
$L1_2$-A_3M (γ'), $D0_{22}$-A_3M (γ"), and $D0_a$-A_3M (δ)	A=Ni, Co, Cr, and Fe and M ($\neq$A)= Ni, Co, Cr, Fe, Al, B, C, Cr, Cu, Hf, La, Mn, Mo, N, Nb, O, P, Re, Ru, S, Si, Ta, Ti, V, W, Y, and Zr
C14-A_2M, A_8M, MC, $(A,M)_6C$, and $(A,M)_{23}C_6$	A, M ($\neq$A)= Ni, Co, Cr, Fe, Al, B, C, Cr, Cu, Hf, La, Mn, Mo, N, Nb, O, P, Re, Ru, S, Si, Ta, Ti, V, W, Y, and Zr
μ-A_6M_7, and σ-A_xM_y	A=Ni, Co, Cr, and Fe and M ($\neq$A) = Al, B, C, Cr, Cu, Hf, La, Mn, Mo, N, Nb, O, P, Re, Ru, S, Si, Ta, Ti, V, W, Y, and Zr
Binary fcc X_xM_{1-x} (γ) at x=0.333, 0.5, 0.625,0.667,0.75, and 0.875	X=Fe, Co, Ni, and Cr, and M= Al, C, Co, Cr, Cu, Fe, Hf, Mn, Mo, Nb, Ni, Re, Si, Ta, Ti, and W
Ternary fcc $X_{1/3}M_{1/3}Z_{1/3}$ and $X_{3/5}M_{1/5}Z_{1/5}$	X=Fe, Co, Ni, and Cr, and M,Z=Al, C, Co, Cr, Cu, Fe, Hf, Mn, Mo, Nb, Ni, Re, Si, Ta, Ti, and W
Binary bcc $M_{1/3}Z_{1/3}$ and ternary bcc $X_{1/3}M_{1/3}Z_{1/3}$.	X=Fe, Co, Ni, and Cr, and M,Z=Al, C, Co, Cr, Cu, Fe, Hf, Mn, Mo, Nb, Ni, Re, Si, Ta, Ti, and W
Binary fcc-based dilute solution Ni_NM at N=31, 107, and 255	M= Al, C, Co, Cr, Cu, Fe, Hf, Mn, Mo, Nb, Ni, Re, Si, Ta, Ti, and W

Table 3: The Alloy Compositions (Weight Percentage) of Taylor and Walsh[30]

Alloy	Ni	Co	Cr	Al	Y	Mo
LN-4	80	0	20	0	0	0
LN-5B	94.4	0	0	4.89	0	0
LN-11	49	22.08	15.54	12.61	0.62	0
LN-21	48.6	22.83	20.01	7.53	0.58	0
LN-33	68.6	0	19.57	10.9	0.41	0
LN-46	53.6	14.82	19.03	11.24	0.43	0.53
LN-49	53	15	19	13	0.5	0.5
LCo-7	0	64	24	12	0.5	0
LCo-22	31.75	39.5	20.17	7.54	0.64	0
LCo-22+Al	29	38	21	11	0.5	0
LCo-29	0.12	74.2	16.94	7.79	0.5	0
LCo-40	0.11	63.7	26.6	8.97	0.54	0
LCo-49	42	28	15	14	0.5	0
TM-309	42	25	23	10	0.5	0
NiCo	57	43	0	0	0	0
Ni	100	0	0	0	0	0

Supplementary Materials

Enhancing the Accuracy and Generality of the Debye–Grüneisen Model: Optimizing the Volume Dependence for Accurate Predictions Across Varied Compositions

Yi Wang,[1,2] Xingru Tan[3], Saro San, [1,2] Shanshan Hu[3], and Michael C. Gao[1]
[1]National Energy Technology Laboratory, 1450 Queen Avenue SW, Albany, OR 97321, USA
[2]NETL Support Contractor, 1450 Queen Avenue SW, Albany, OR 97321, USA
[3] Mechanical & Aerospace Engineering Department, Benjamin M. Statler College of Engineering and Mineral Resources, West Virginia University, Morgantown, WV 26505, USA

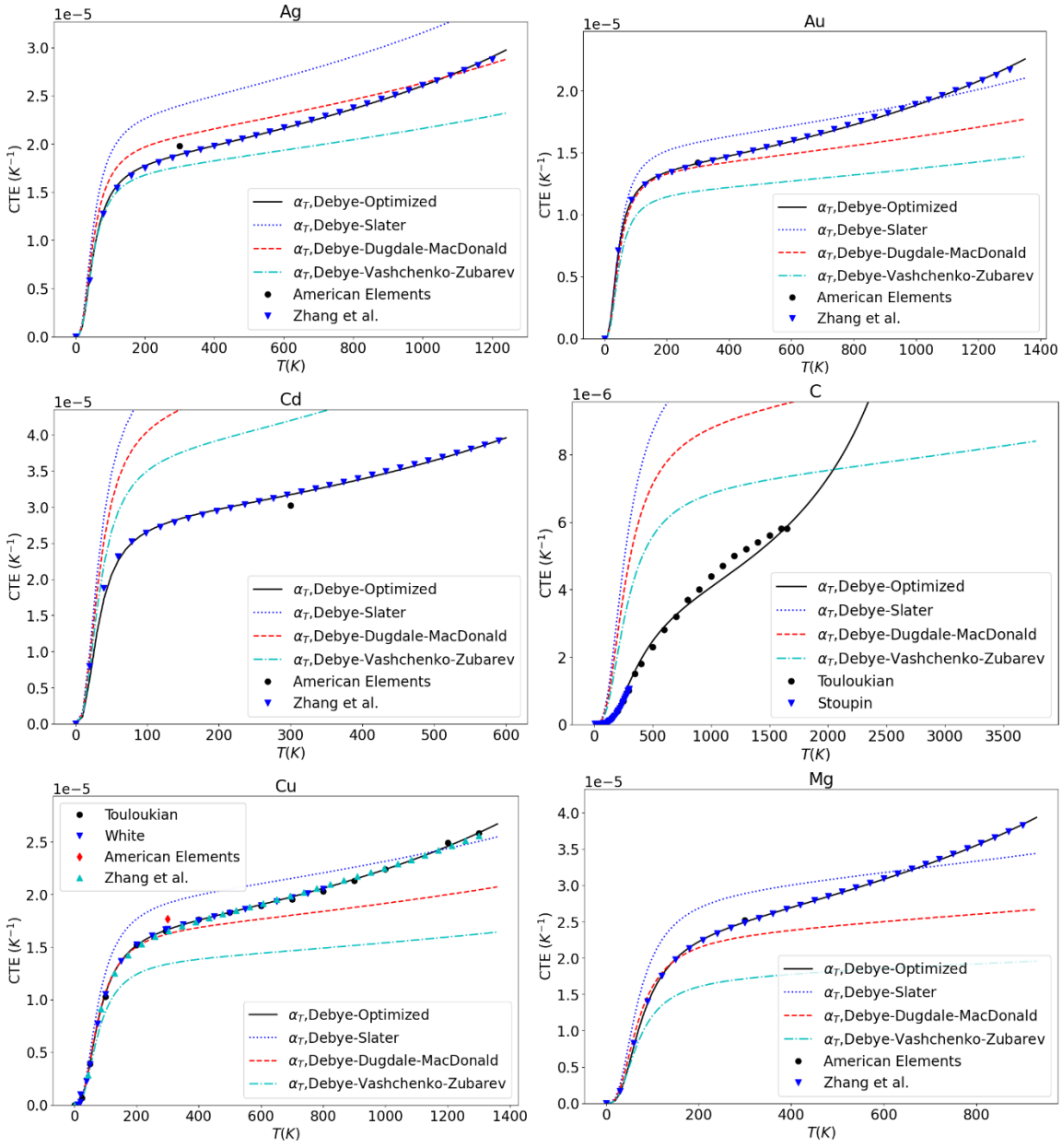

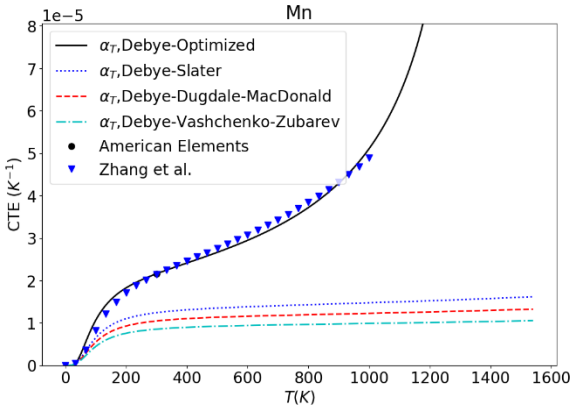
Mn
1e−5
CTE (K^{-1})
$T(K)$
α_T,Debye-Optimized
α_T,Debye-Slater
α_T,Debye-Dugdale-MacDonald
α_T,Debye-Vashchenko-Zubarev
American Elements
Zhang et al.

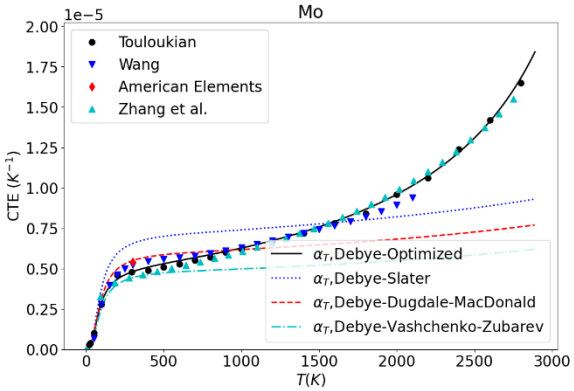
Mo
1e−5
CTE (K^{-1})
$T(K)$
Touloukian
Wang
American Elements
Zhang et al.
α_T,Debye-Optimized
α_T,Debye-Slater
α_T,Debye-Dugdale-MacDonald
α_T,Debye-Vashchenko-Zubarev

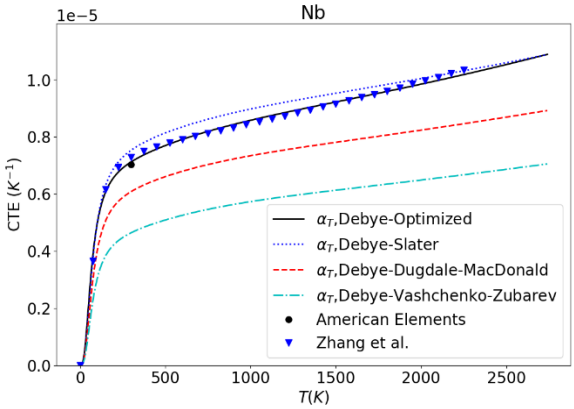
Nb
1e−5
CTE (K^{-1})
$T(K)$
α_T,Debye-Optimized
α_T,Debye-Slater
α_T,Debye-Dugdale-MacDonald
α_T,Debye-Vashchenko-Zubarev
American Elements
Zhang et al.

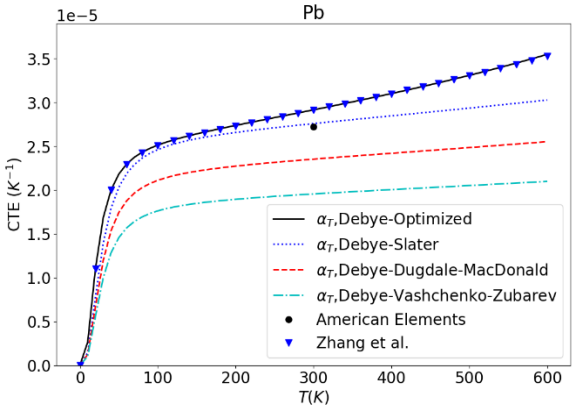
Pb
1e−5
CTE (K^{-1})
$T(K)$
α_T,Debye-Optimized
α_T,Debye-Slater
α_T,Debye-Dugdale-MacDonald
α_T,Debye-Vashchenko-Zubarev
American Elements
Zhang et al.

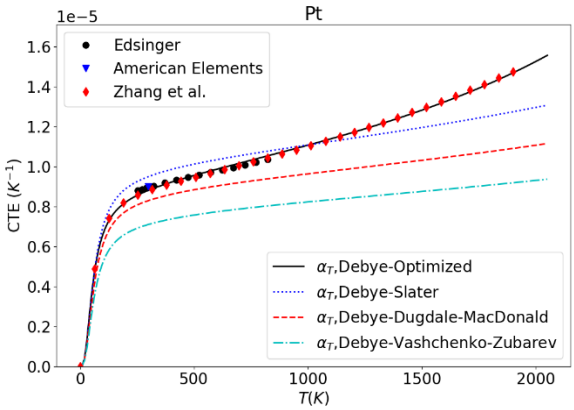
Pt
1e−5
CTE (K^{-1})
$T(K)$
Edsinger
American Elements
Zhang et al.
α_T,Debye-Optimized
α_T,Debye-Slater
α_T,Debye-Dugdale-MacDonald
α_T,Debye-Vashchenko-Zubarev

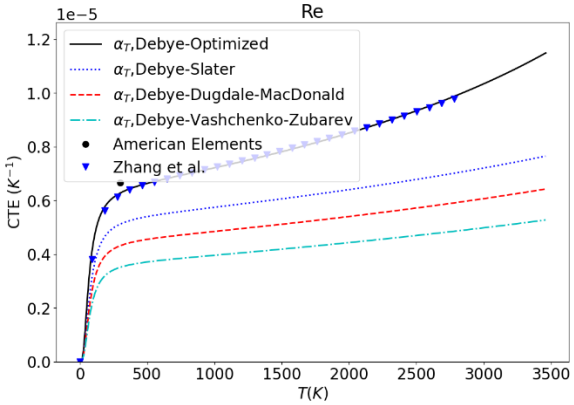
Re
1e−5
CTE (K^{-1})
$T(K)$
α_T,Debye-Optimized
α_T,Debye-Slater
α_T,Debye-Dugdale-MacDonald
α_T,Debye-Vashchenko-Zubarev
American Elements
Zhang et al.

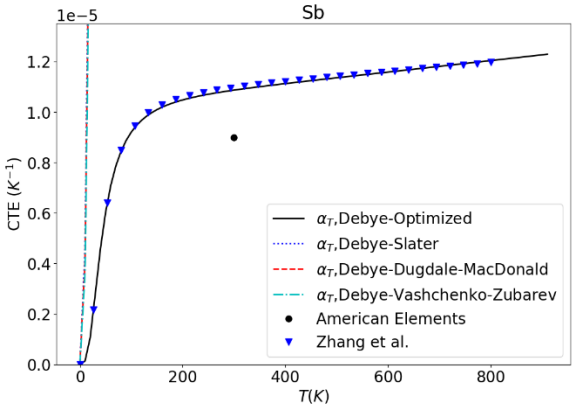
Sb
1e−5
CTE (K^{-1})
$T(K)$
α_T,Debye-Optimized
α_T,Debye-Slater
α_T,Debye-Dugdale-MacDonald
α_T,Debye-Vashchenko-Zubarev
American Elements
Zhang et al.

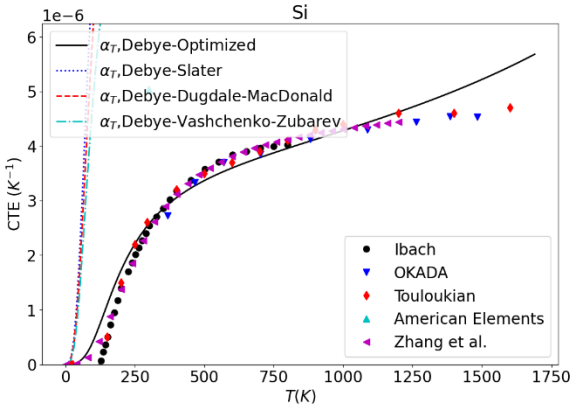
Si
1e−6
CTE (K^{-1})
$T(K)$
α_T,Debye-Optimized
α_T,Debye-Slater
α_T,Debye-Dugdale-MacDonald
α_T,Debye-Vashchenko-Zubarev
Ibach
OKADA
Touloukian
American Elements
Zhang et al.

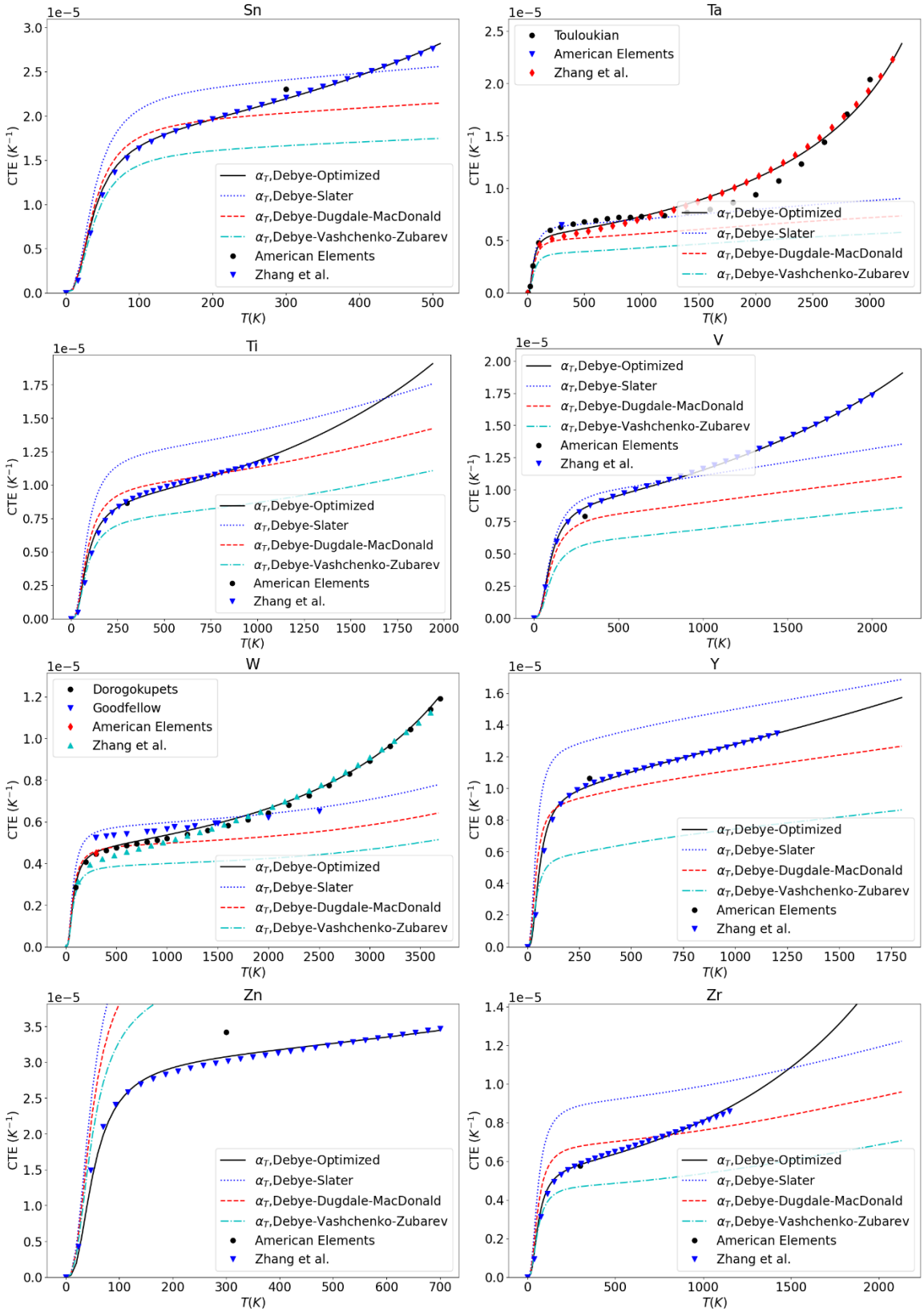

Figure S1. Comparison of the true linear coefficient of thermal expansion (α_T) described by the present optimized Debye-Grüneisen model with the Moruzzi model [1] employing the Grüneisen

parameters determined by the Slater [2], Dugdale-MacDonald [3], and Vashchenko-Zubarev [4] expressions. The dots plotted in the left panels represent the experimental CTEs for pure elements: Ag, Au, Cd, C, Cu, Mg, Mn, Mo, Nb, Pb, Pt, Re, Sb, Si, Sn, Ta, Ti, V, W, Y, Zn, and Zr.

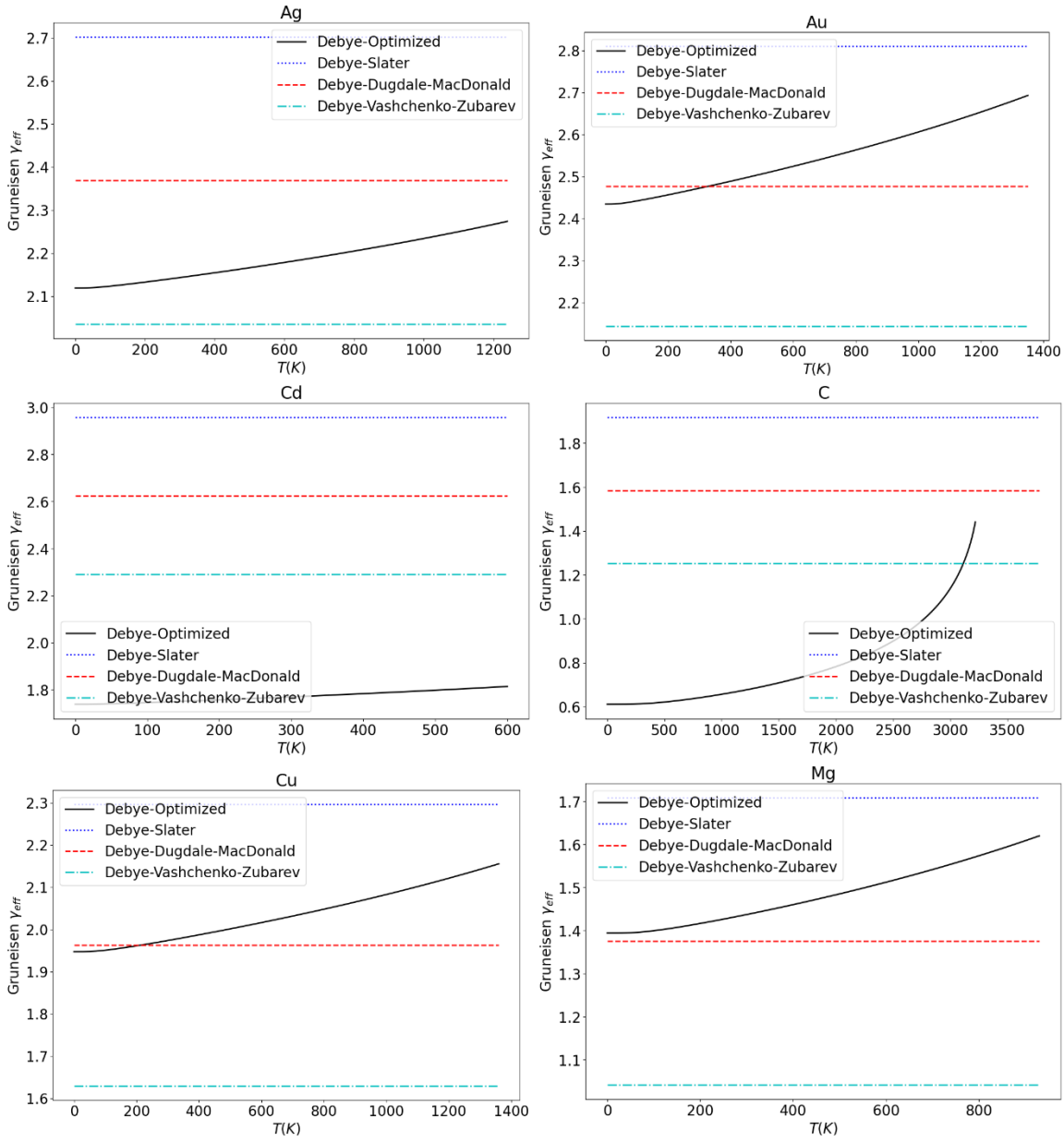

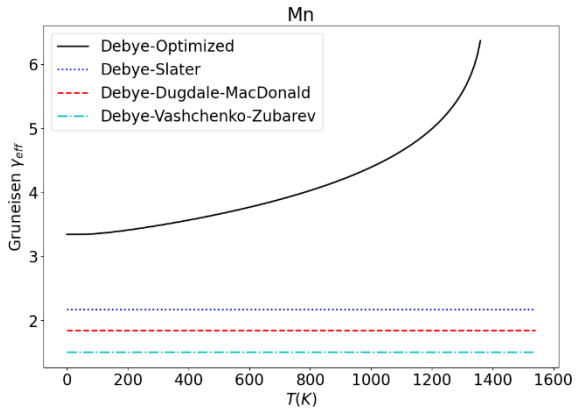
Mn
Debye-Optimized
Debye-Slater
Debye-Dugdale-MacDonald
Debye-Vashchenko-Zubarev
Gruneisen γ_{eff}
$T(K)$

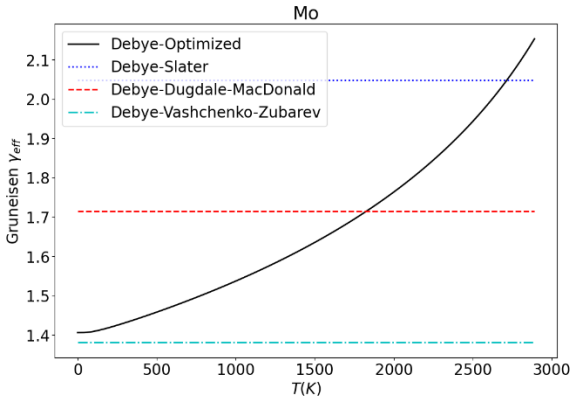
Mo
Debye-Optimized
Debye-Slater
Debye-Dugdale-MacDonald
Debye-Vashchenko-Zubarev
Gruneisen γ_{eff}
$T(K)$

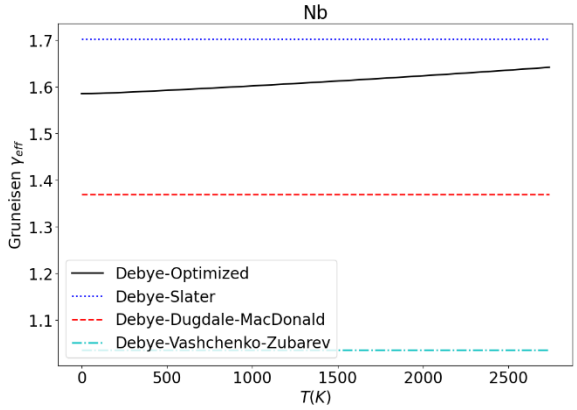
Nb
Debye-Optimized
Debye-Slater
Debye-Dugdale-MacDonald
Debye-Vashchenko-Zubarev
Gruneisen γ_{eff}
$T(K)$

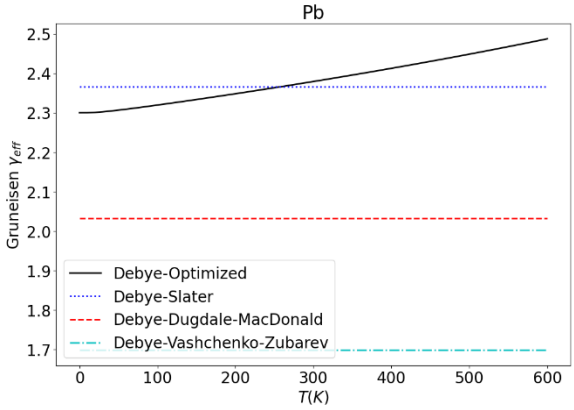
Pb
Debye-Optimized
Debye-Slater
Debye-Dugdale-MacDonald
Debye-Vashchenko-Zubarev
Gruneisen γ_{eff}
$T(K)$

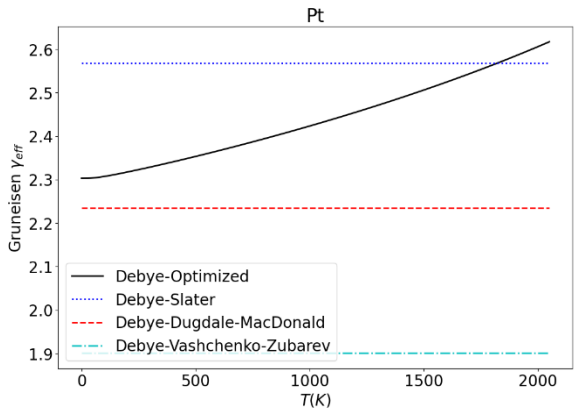
Pt
Debye-Optimized
Debye-Slater
Debye-Dugdale-MacDonald
Debye-Vashchenko-Zubarev
Gruneisen γ_{eff}
$T(K)$

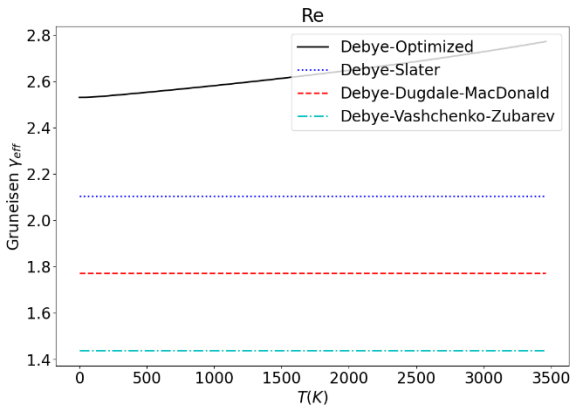
Re
Debye-Optimized
Debye-Slater
Debye-Dugdale-MacDonald
Debye-Vashchenko-Zubarev
Gruneisen γ_{eff}
$T(K)$

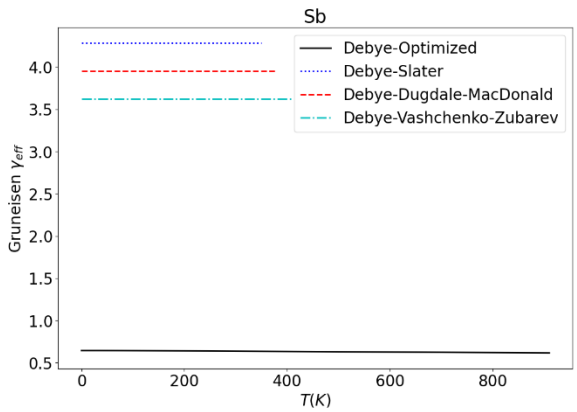
Sb
Debye-Optimized
Debye-Slater
Debye-Dugdale-MacDonald
Debye-Vashchenko-Zubarev
Gruneisen γ_{eff}
$T(K)$

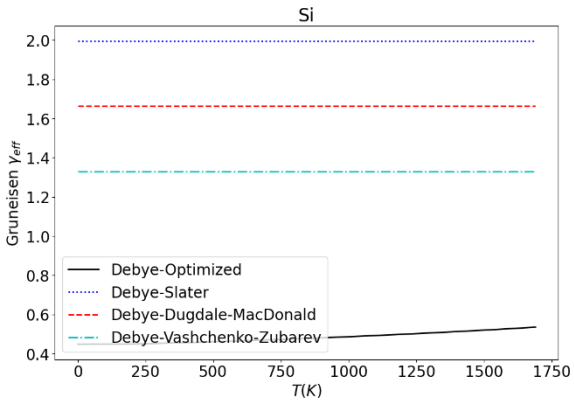
Si
Debye-Optimized
Debye-Slater
Debye-Dugdale-MacDonald
Debye-Vashchenko-Zubarev
Gruneisen γ_{eff}
$T(K)$

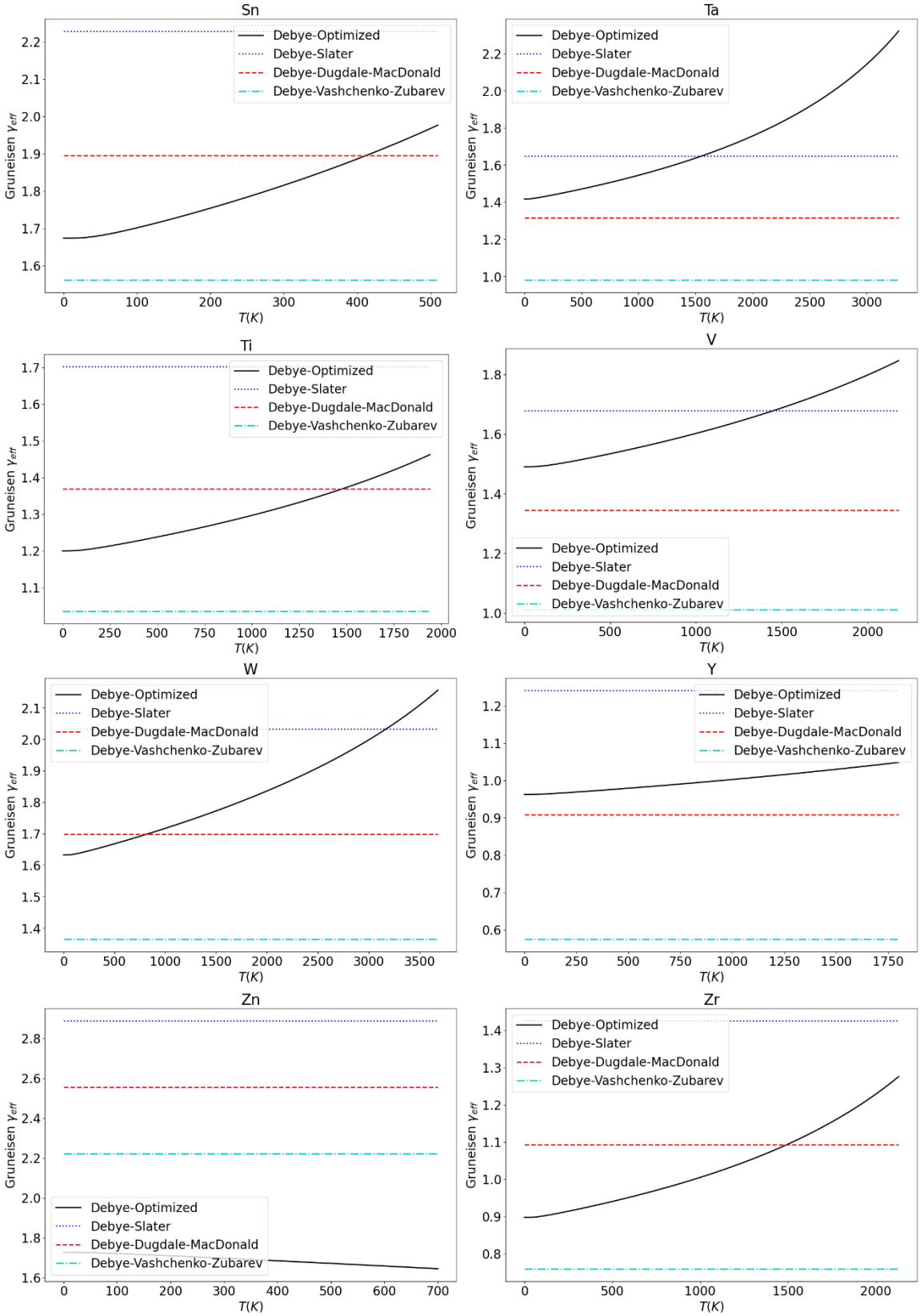
Sn
Ta
Ti
V
W
Y
Zn
Zr
Debye-Optimized
Debye-Slater
Debye-Dugdale-MacDonald
Debye-Vashchenko-Zubarev
Gruneisen γ_{eff}
$T(K)$

Figure S2. Comparison of the effective Grüneisen parameters (γ_{eff}, see Eq. 5 in the main text) described by the present optimized Debye-Grüneisen model with the Moruzzi model [1] employing the Grüneisen parameters determined by the Slater [2], Dugdale-MacDonald [3], and Vashchenko-Zubarev [4] expressions for pure elements: Ag, Au, Cd, C, Cu, Mg, Mn, Mo, Nb, Pb, Pt, Re, Sb, Si, Sn, Ta, Ti, V, W, Y, Zn, and Zr.

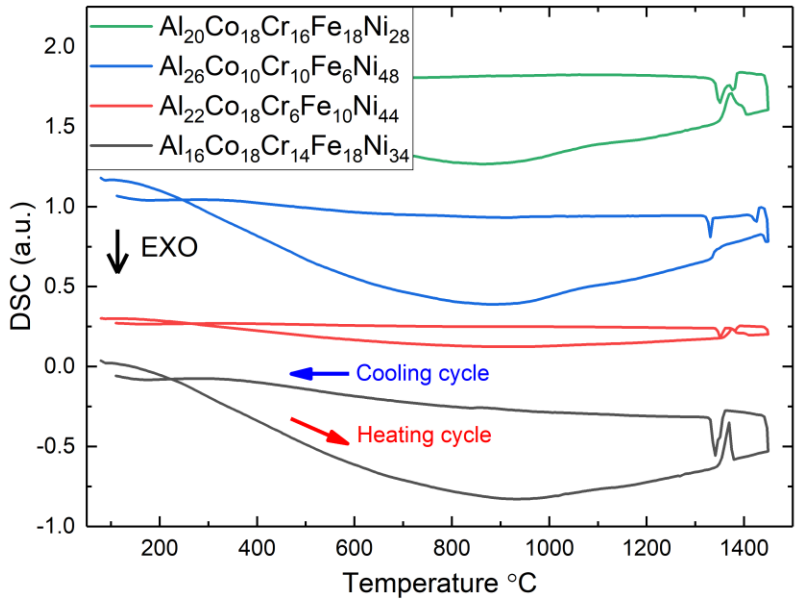

Figure S3. DSC measurement.

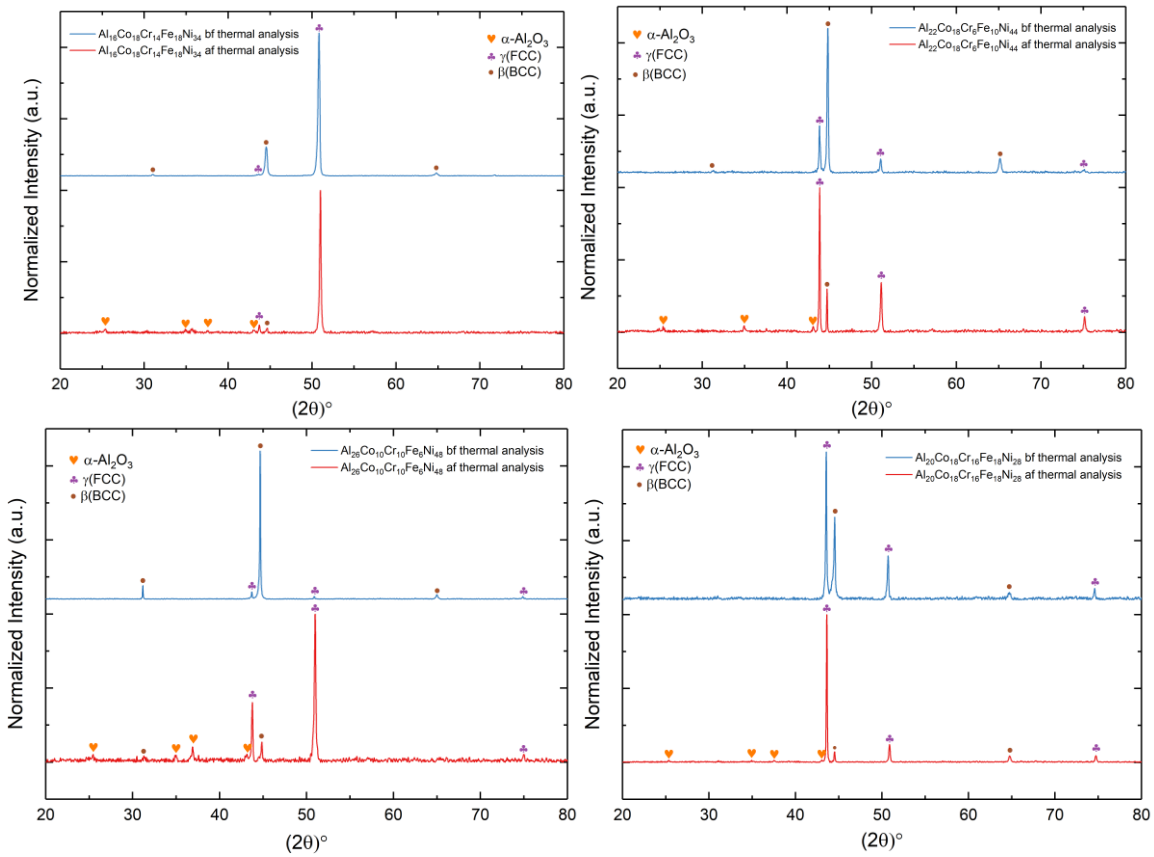

Figure S4. XRD results for four samples before and after CTE measurement.

(a) (b)

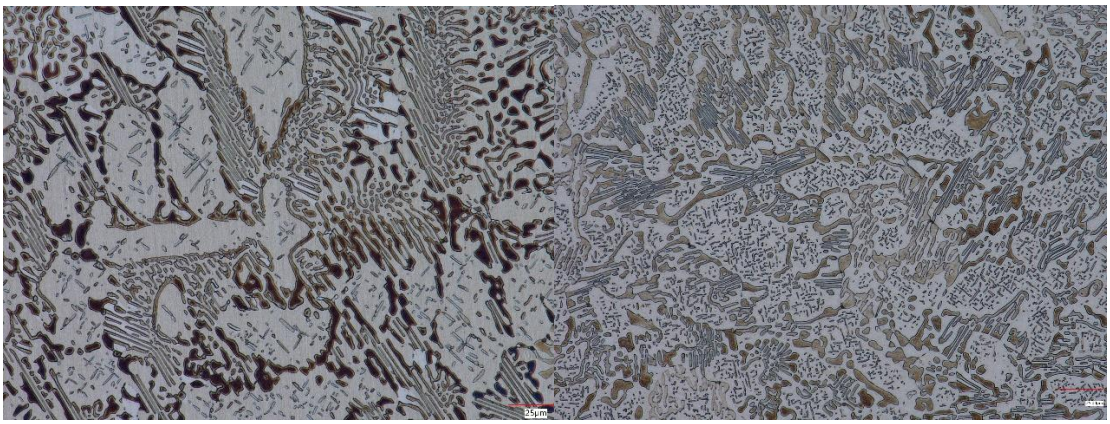

Figure S5. Microstructure (a) before and (b) after CTE measurement for Al16Co18Cr14Fe18Ni34.

(a) (b)

Figure S6. Microstructure (a) before and (b) after CTE measurement for Al22Co18Cr6Fe10Ni44.

(a) (b)

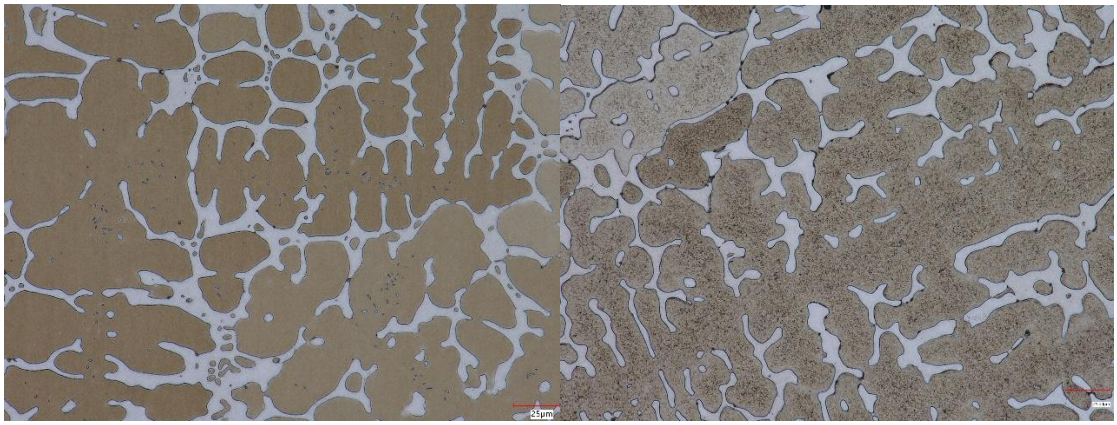

Figure S7. Microstructure (a) before and (b) after CTE measurement for Al26Co10Cr10Fe6Ni48.

(a) (b)

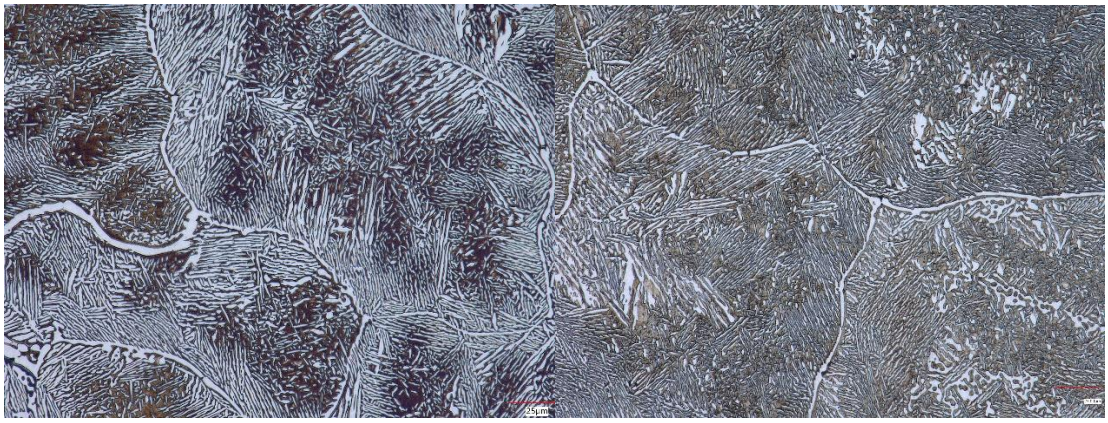

Figure S8. Microstructure (a) before and (b) after CTE measurement for Al16Co18Cr14Fe18Ni34.

The attached cvs files contain the calculated mean and true CTE values for 90,000 Al-Co-Cr-Fe-Ni alloys at 1000 °C, 1050 °C, 1100 °C, 1150 °C, and 1200 °C.

References

[1] V.L. Moruzzi, J.F. Janak, K. Schwarz, Calculated thermal properties of metals, Physical Review B 37(2) (1988) 790-799.
[2] J.C. Slater, Introduction to chemical physics, Read Books Ltd2011.
[3] Y. Wang, R. Ahuja, B. Johansson, Mean-field potential approach to the quasiharmonic theory of solids, Int. J. Quantum Chem. 96 (2004) 501-506.
[4] V.Y. Vashchenko, V. Zubarev, Concerning the Grüneisen constant, Sov. Phys. Solid. State 5 (1963) 653-655.